Nanowire arrays as cell force sensors to investigate adhesin-enhanced holdfast of single cell bacteria and biofilm stability

Sahoo, Prasana K.; Janissen, Richard; Monteiro, Moniellen P.; Cavalli, Alessandro; Murillo, Duber M.; Merfa, Marcus V.; Cesar, Carlos L.; Carvalho, Hernandes F.; De Souza, Alessandra A.; Bakkers, Erik P.A.M.

DOI
10.1021/acs.nanolett.6b01998

Publication date
2016

Document Version
Accepted author manuscript

Published in
Nano Letters: a journal dedicated to nanoscience and nanotechnology

Citation (APA)
Sahoo, P. K., Janissen, R., Monteiro, M. P., Cavalli, A., Murillo, D. M., Merfa, M. V., Cesar, C. L., Carvalho, H. F., De Souza, A. A., Bakkers, E. P. A. M., & Cotta, M. A. (2016). Nanowire arrays as cell force sensors to investigate adhesin-enhanced holdfast of single cell bacteria and biofilm stability. *Nano Letters: a journal dedicated to nanoscience and nanotechnology*, *16*(7), 4656-4664. https://doi.org/10.1021/acs.nanolett.6b01998

Important note
To cite this publication, please use the final published version (if applicable).
Please check the document version above.

Nanowire arrays as cell force sensors to investigate adhesin-enhanced holdfast of single cell bacteria and biofilm stability

Prasana. K. Sahoo[1], Richard Janissen[1,2], Moniellen P. Monteiro[1], Alessandro Cavalli[3], Duber M. Murillo[1], Marcus V. Merfa[4], Carlos L. Cesar[5], Hernandes F. Carvalho[6], Alessandra A. de Souza[4], Erik P.A.M. Bakkers[3], Monica A. Cotta[1,]*

[1]Applied Physics Department, Institute of Physics 'Gleb Wataghin', State University of Campinas, 13083-859, Campinas, São Paulo, Brazil

[2]Kavli Institute of Nanoscience, Delft University of Technology, 2629 HZ Delft, The Netherlands

[3]Applied Physics Department, Eindhoven University of Technology, 5600 MB Eindhoven, The Netherlands

[4]Citrus Center APTA 'Sylvio Moreira', Agronomic Institute of Campinas, 13490-970, Cordeirópolis, São Paulo, Brazil

[5]Quantum Electronics Department, Institute of Physics 'Gleb Wataghin', State University of Campinas, 13083-859, Campinas, São Paulo, Brazil

[6]Structural and Functional Biology Department, Institute of Biology, State University of Campinas, 13083-865, Campinas, São Paulo, Brazil

KEYWORDS: Bacterial biofilm; nanowire arrays; force sensor; adhesin; cell adhesion; *Xylella fastidiosa*

ABSTRACT

Surface attachment of a planktonic bacteria, mediated by adhesins and extracellular polymeric substances (EPS), is a crucial step for biofilm formation. Some pathogens can modulate cell adhesiveness, impacting host colonization and virulence. A framework able to quantify cell-surface interaction forces and their dependence on chemical surface composition may unveil adhesiveness control mechanisms as new targets for intervention and disease control. Here we employed InP nanowire arrays to dissect factors involved in the early stage biofilm formation of the phytopathogen *Xylella fastidiosa*. *Ex-vivo* experiments demonstrate single-cell adhesion forces up to 45 nN, depending on the cell orientation with respect to the surface. Larger adhesion forces occur at the cell poles; secreted EPS layers and filaments provide additional mechanical support. Significant adhesion force enhancements were observed for single cells anchoring a biofilm and particularly on XadA1 adhesin-coated surfaces, evidencing molecular mechanisms developed by bacterial pathogens to create a stronger holdfast to specific host tissues.

Single cell bacterial adhesion to a surface is the first, and critical, step to originate a biofilm. After a community of attached microorganisms is formed, it embeds itself in a matrix of hydrated extracellular polymeric substances (EPS), which includes a variety of biomolecules, such as DNA, oligopeptides, proteins, lipids and lipopolysaccharides.[1-5] EPS secretion represents an important factor for the motile- to sessile-stage transition during bacterial cell adhesion. Furthermore, specific extracellular components often facilitate adhesion by reducing the energy barrier formed between approaching surfaces,[6-8] in a process which depends mostly on bacteria-host adaptation mechanisms.[9-10]

Thus, it is important to probe the specific dependence of bacterial cell adhesion on surface chemical composition and the corresponding molecular mechanisms. EPS-mediated adhesion is also noteworthy of similar studies; after initial cell attachment, the secreted EPS eventually accumulates, leading to changes in biofilm stiffness and elasticity. In that sense, a quantitative analysis of cell-surface interaction mechanisms may eventually lead to new strategies for biofilm eradication, a serious technological challenge in several and very different areas, such as health care and agriculture.[1,3,5,11] Further complexity to the scenario of bacterial biofilm infection arises from the ability of many species to modulate cell adhesiveness, and hence host colonization, in response to changing environmental conditions.[12] In fact, bacterial cells respond to many cues from the surface such as wettability[13,14], chemical composition[15], compliance[16,17] and

nanotopography.[18-23] Nanostructure spacing on the surface is a key issue, particularly when the characteristic dimensions of the array are in the same scale of the cells.[22] Nanopillar[22,23] and nanowire arrays[24-27] modulate bacterial motility, cell angular orientation upon adhesion, and cell replication, surpassing the importance of other microenvironmental parameters.[25-27]

However, the molecular mechanisms of bacterial cell adhesion, which are triggered by nanotopography, have not been fully addressed yet. Accurate investigation of such interplay could be achieved by quantitatively measuring and probing the adhesion forces of cells. Over the past decade, accurate quantitative investigation of the adhesion forces of eukaryotic and prokaryotic cell types have been realized by different techniques.[28-38] Force measurements are mostly based on force-induced deformations of the sensing components; for different types of bacteria, the reported adhesion forces range from few piconewtons to several micronewtons in magnitude[32-38]. However, each technique presents certain limitations towards the accuracy and statistics of the measurement methodology. Stiffer and more uniform materials, such as semiconductor-based nanowire arrays, pose as an interesting alternative. The deflection of nanowires positioned in geometrically-controlled arrays has been used so far to probe forces present during surface interactions of mammalian cells[30] or to evaluate their intracellular processes while adhered to a substrate.[39] Despite the possibility of piconewton resolution in force measurements,[30] this methodology has not been extended yet to adhesion studies of prokaryotic cells, with smaller spatial dimensions. Moreover, no quantitative studies have determined the relation between single cell and biofilm adhesion forces and their dependence on the chemical surface composition.

Addressing these issues will be strongly facilitated if the adhesion stages of a bacterial species upon biofilm formation are already documented. This is the case of *Xylella fastidiosa*, which is among the top ten most studied phytopathogens.[12,40,41] This bacterium forms biofilms in xylem vessels, causing water and nutrition stress in plants, affecting several types of crops worldwide and causing substantial economic losses.[42] Recently, the *X. fastidiosa* biofilm formation process has been examined at single cell resolution for a bacterial strain affecting citrus plants; this study has also pointed out spatiotemporal changes in EPS composition along the bacterial life cycle.[41] In addition to EPS, *X. fastidiosa* expresses several types of extracellular adhesins at the cell membrane; previous studies have identified the expression of transmembrane trimeric autotransporter adhesins (TAA), such as XadA, during the entire biofilm formation process. [43] In particular, XadA1 is an extracellular TAA which has been extensively studied in literature about

Xylella fastidiosa due to its role in biofilm formation and outer membrane vesicles (OMVs),[43-45] features that have important implications in bacterial fitness and pathogenicity. These OMVs, usually produced by Gram-negative bacteria, contain biologically active molecules and regulate many cell functions, from virulence and metabolism to community communication.[44-49] Despite XadA1 expression during most of *X. fastidiosa* life cycle, the role of this adhesin in OMVs during biofilm formation remains elusive. Elucidating this question is particularly relevant to *X. fastidiosa* as the bacteria inhabit both plants and insect vectors alike. As these hosts exhibit very different surface compositions and structures, the efficiency of single cell adhesion on each case might implicate tremendous plasticity of adhesion capacity and mechanism.

In this work, we employed spatially ordered InP nanowire arrays to evaluate *X. fastidiosa* single cell adhesion forces and explore their dependence on organochemical surface compositions. Quantitative measurements of cell adhesion forces were obtained by observing the displacement of nanowire tip positions upon cell attachment, using field-emission scanning electron microscopy (FESEM) and confocal laser scanning fluorescence microscopy (CLSM). *Ex-vivo* measurements during bacterial growth in the first stages of biofilm formation were acquired at the CLSM. We detected forces in nanonewton range during interaction and adhesion of individual *X. fastidiosa* cells to InP nanowire arrays, with spacing similar to the bacterial cell diameter (~ 500 nm, **Fig. S1**). The measured force range and spatial cell distribution depended on the orientation assumed by the cell upon interaction with the nanowires, as well as on its motility degree upon attachment. For nanowire arrays functionalized with XadA1 adhesins, we observed up to a two-fold increase in adhesion forces, in similar bacterial growth conditions. A comparable range of adhesion forces was observed for single cells attached to the non-functionalized nanowires while anchoring a small biofilm.

InP nanowire arrays used in this work were grown by low-pressure Metalorganic Vapor Pressure Epitaxy (MOVPE) on (111) InP substrates with the vapor-liquid-solid (VLS) method. The 90 nm nanowire diameter was defined by the amount of Au catalyst obtained by nanoimprint technique. Nanowires grew vertically, perpendicular to the substrate, in the <111> direction, with 1500 nm as typical length. Prior to covalent XadA1 protein attachment, InP samples were cleaned and oxygen plasma treated, followed by functionalization with ethanolamine and PEGylation. All adhesion experiments used *Xylella fastidiosa* inoculum in Periwinkle Wilt (PW) broth media with a concentration of 1×10^7 CFU mL^{-1}. InP nanowire arrays were incubated in a chamber with 400

µl of inoculum at 28 °C. After defined growth times, the whole system was taken for *ex-vivo* CLSM measurements or FESEM studies. In the latter case, the constituents of the culture media and non-attached biofilms were removed by gentle washing. For the *ex-vivo* CLSM measurements, both the magnitude and orientation of the deflection of nanowires, determined from their tip positions in the times series, were analyzed using the ImageJ software and translated into forces, according to the methodology described by Hallstrom *et al.*[30] The estimated maximum force within linear elasticity approximation for our nanowires is 75 nN. A thorough description of materials and methods used in this work is provided as Supporting Information.

The effect of the array nanotopography on *X. fastidiosa* adhesion was first evaluated from FESEM images of dry samples. Despite surface tension effects due to water removal,[50] dehydrated samples allowed us to extend the concept of force measurement using nanowires to prokaryotes and probe their force ranges, as well as those from EPS filaments. **Figure 1** shows striking differences in attachment orientation for bacterial cells adhered to flat InP substrates (**Fig. 1A**) and to the InP nanowire array (**Fig. 1B**). Flat substrates exhibited random cell distribution and orientation on the surface, with few clusters. In contrast, on the nanostructured substrate, single cells were attached at the bottom surface within the vicinity of the nanowires, in most cases aligned with them (see also **Fig. S2**). Widefield fluorescence microscopy (WFM, **Fig. 1C**) measurements provide a larger field of view, where a spatial pattern of vertically and horizontally aligned Green Fluorescent Protein (GFP)-expressing *X. fastidiosa* cells can be readily distinguished. Cell-cell contact is essentially mediated through bacterial poles, in agreement with previous reports.[41] Furthermore, FESEM images (**Fig. 1A, B**) show a difference in contrast around the cells (colorized in green), particularly at the poles, which is an indication of soluble EPS secretion (viewed as the black cell contour).[41,51] These cells are apparently dehydrated, and their rod shapes are not perfectly preserved during the drying process under N_2 flow.

A non-negligible fraction (up to 5%) of the cells, however, adhered horizontally close to the top of the nanowires, instead of to the bottom surface (**Fig. 1D)**. The rod shape of the cell is better preserved, showing signs of soluble EPS coverage at the attachment regions (**Fig. S3**). An asymmetric bending of the nanowires in contact with this cell is explicitly observable. The magnitude of the nanowire tip position displacement caused by the interaction with the cell can be measured in top view FESEM images (**Fig. 1E**), and translated into forces[30] (see Materials &

Methods in SI). The polar plot in the inset shows the force magnitude and directions applied to each cell-attached nanowire in the FESEM image (**Fig. 1E**).

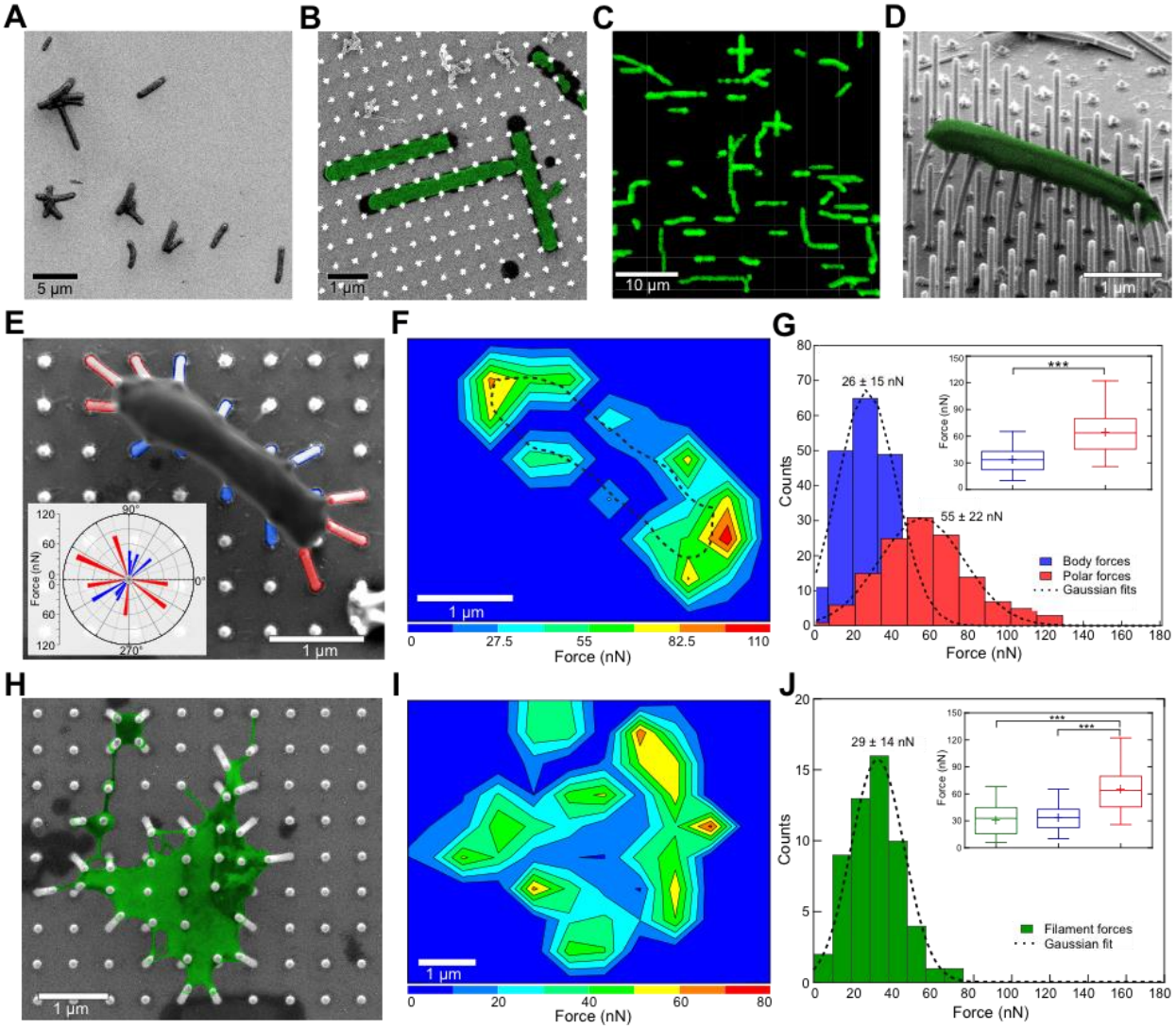

Figure 1. Effect of nanotopography and force range evaluation on dry samples with adhered GFP-expressing *X. fastidiosa* 11399 strain cells. FESEM images of cells adhered to (**A**) pristine, flat InP surface and (**B**) to spatially ordered array of nanowires (viewed as the white dots in the image; cells colorized in green and EPS shown in its original black color). (**C**) WFM image of *X. fastidiosa* cells (in green) adhered to the nanowire array. (**D**) FESEM image showing the deformation of nanowires in direct contact with the attached cell body (colorized in green). (**E**) Top view FESEM image of bacteria adhered to nanowires, showing the tip displacements; the inset exhibits a polar plot of force magnitude and direction for each cell-attached nanowire. (**F**) Spatial distribution of deflection forces measured in (E) (corresponding bacteria shape overlaid as dashed line). (**G**) Distribution of measured forces derived from the deformation of the nanowires by bacterial cells from body (*n = 197*) and polar (*n = 130*) regions (*n* = number of nanowires measured in each case). (**H**) FESEM image showing EPS layer fragment and emanating filaments from a single cell (colorized in green, along with EPS). (**I**) spatial distribution of deflection forces measured in (**H**). (**J**) Distribution of forces derived from the deformation of the nanowires by EPS layer and emanating filaments (*n* = 70). All samples analyzed here were grown for 24 h, except for that shown in (**H**), for which growth time was 168 h. For box plots shown as insets in (**G**) and (**J**), we performed one-way, two-tailed ANOVA with subsequent Tukey post-hoc test to compare the force values and their statistical difference; the asterisks state significance level of *p = 0.0001*.

The spatial distribution of measured forces for a single cell (**Fig. 1F**) presents larger values at the poles than alongside the cell body. The statistical distribution (**Fig. 1G**) shows that the difference between the average force in the region of the poles (55 ± 22 nN) and the cell body (26 ± 15 nN), measured for $n = 327$ individual nanowires, is significant (two-tailed T-test, $p = 0.0001$) by a factor of two. The same methodology can also be applied to secreted EPS layers and filaments, as illustrated in **Fig. 1H**. These structures have been suggested to provide mechanical stability to the biofilm within the living environment.[5,41] In fact, the spatial distribution of force values (**Fig. 1I**) shows that even very thin filaments (~ 50 nm wide) of the elongated EPS layer (**Fig. 1H**) can exert large forces, up to ~ 70 nN at the position where they are connected to the nanowires. The statistical analysis for a larger ensemble of EPS structures demonstrate that the average force of 29 ± 14 nN (**Fig. 1J**) is comparable to that observed alongside the cell body. Despite possible surface tension effects, these results show statistically significant, normal-distributed force values from measuring several bacterial samples.

This result suggests that irreversible cell attachment to nanowires at this biofilm formation stage is based on an EPS-mediated mechanism. We thus proceeded to investigate the range of cell adhesion forces in growth media and liquid environments, by carrying out CLSM *ex-vivo* measurements with GFP-expressing *X. fastidiosa* cells (**Fig. 2**, **Fig. S4**, and **Supplementary video MV1**). The positions of the nanowire tips were measured by the reflected intensity of the CLSM laser emission line (488 nm), while the single bacterial cell attached to the nanowire surface was monitored by the GFP emission. Both nanowire tip and single cell positions were recorded over time. The focus of the microscope during the experiment was kept in the plane containing the nanowire tips, and any cells attached to them. The depth of the confocal volume is set to about the same size as the cell average diameter (**Fig. S1**). The acquisition time was limited to 60 seconds, before complete photobleaching of the intracellular GFP took place. All *ex-vivo* experiments were conducted with no external flow.

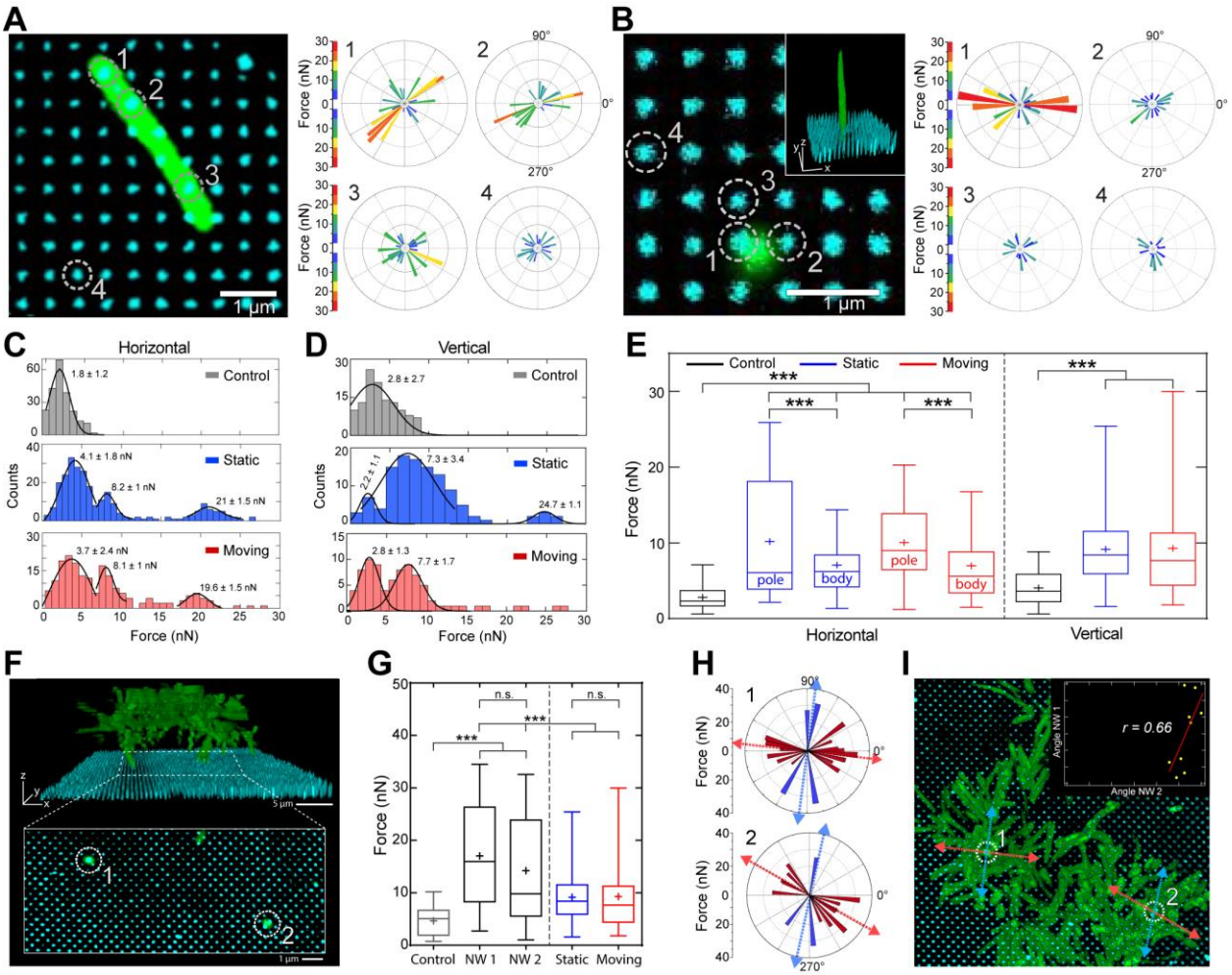

Figure 2. ***Ex-vivo*** **force measurements for single cells.** The CLSM images show GFP-expressing *X. fastidiosa* cells adhered to InP nanowires in (**A**) horizontal and (**B**) vertical orientations (the images show the fluorescence of GFP and the reflected laser intensity at the nanowire tip) and corresponding polar plots of force and direction for individual nanowires (marked by dashed circles and numbered in the corresponding image). The distribution of force values for horizontal static and moving adhered bacteria is shown in (**C**), along with the control measurements. Similarly, (**D**) shows the distribution of forces for vertical cell orientations, with the corresponding control. Tukey boxplot of the overall force values for the cell polar region (pole) and cell body (body) (**E**) measured for (**A-D**) with the statistical results of one-way ANOVA and comparison via Tukey post-hoc test with significance level of $p = 0.0001$. The statistics and number of cell adhesion forces measured for each orientation in (**C**), (**D**), and (**E**) are summarized in **Table S1**. 3D CLSM image (**F**) showing a small biofilm and two nanowires with vertically adhered bacteria, anchoring the cells to the surface. Tukey boxplot (**G**) shows the force values measured for the two nanowires ($n = 42$ for NW1, NW2 and control) highlighted in (**F**), with significant variation in force values when compared to individual single cells (one-way ANOVA and comparison via Tukey post-hoc test with $p = 0.0001$). Polar plots (**H**) show the magnitude and direction of the forces calculated for the two nanowires in (**F**) with arrows indicating the predominant, average direction of movement; the noise was excluded by considering only forces with values larger than control+10%. (**I**) CLSM top view image of the small biofilm, with the marked position of the two nanowires (as in **F**) and the average directions shown in (**H**). The inset shows the Pearson correlation ($r = 0.66$) of motion angular directions of the two nanowires featured in (**F**) occurring in the same time interval. All samples analyzed here were grown for 24 h prior to CLSM experiments.

The *ex-vivo* CLSM images in **Fig. 2 (A, B)** illustrate two typical orientations assumed by the cells adhered to the nanowires, either lying horizontally or standing upright (henceforth called 'horizontal' and 'vertical'). For both orientations, cells could be either 'static' or 'moving'; in the latter case, the cell pole position was fixed by attachment to one or more nanowires, while the cell body moved over time (**Supplementary videos MV2 to MV5**). The polar plots in **Fig. 2 (A, B)** exhibit the adhesion force magnitude and direction calculated from the deflection of the nanowires marked and numbered in the corresponding images. The horizontal cell adhered to at least three nanowires and remained relatively motionless, or 'static' (**Fig. 2A**). For the vertically oriented cell, its polar region is observable in **Fig. 2B**, attached to a nanowire, with the 3D image of the full cell in the figure inset. A precession-like body motion was observed during the experiment, in this 'moving' configuration (**Supplementary video MV4**). In each experiment, a nanowire away from the cell was used as control; we have determined experimentally that noise limits the detection of force values below 5 nN (**Fig. S4**). In the case of the horizontal, static cell (**Fig. 2A**), we observe that three nanowires demonstrated larger deflection forces than the control. However, the nanowire at position 1, attached near the cell pole, showed significantly larger force values, up to ~ 23 nN, and probably represents the initial adhesion point of the cell. Despite the difference in nominal force values, these results agree qualitatively with our FESEM data. Vertical bacteria, however, can not be found in dried samples; the cells may collapse on the surface upon media removal. *Ex-vivo* measurements for vertical bacteria showed that the closest nanowire to the polar region, and to which the cell is probably adhered to, presented significantly larger force values (up to ~ 30 nN) compared to neighboring nanowires (**Fig. 2B**). Additionally, from a more general perspective, the force amplitude variation over time for both static and moving cases of horizontally (**Fig. S5A**) and vertically (**Fig. S5B**) oriented cells show significant differences regarding the average forces for the control nanowires in the experiment.

The overall force distribution for a larger ensemble of bacterial cells, in different types of configuration, is summarized in **Fig. 2C, D**. In either horizontal or vertical configurations, the histograms suggest multimodal distributions, and thus a stiffer material. The relative immobility of the cell, particularly in the 'horizontal' orientation, is consistent with the presence of EPS along the cell body, making it more permanently attached to the nanowire. For the vertical cells, where mainly the polar region is attached to the nanowires, broader force distributions were observed.

Interestingly, our experiments also reveal the impulse transferred to the nanowire upon short-time contact with the cell membrane, as evidenced in **Fig. S6** and **Supplementary video MV3**.

Bacterial adhesion forces to the nanowires reached values, ~ 30 nN, up to 6 times above noise levels (**Fig. 2E**; see also **Table S1**), with statistically significant differences from the control. Furthermore, larger forces are observed for nanowires attached to cell poles for both static and moving horizontal bacteria, with values comparable to those from vertical cells. This result strongly supports previously reported data that initial adhesion takes place through the bacterial pole, even though the cells eventually lay down on the surface.[41]

The determination of single cell adhesion strength is even more important due to the architecture of *X. fastidiosa* biofilms, which are floating structures held to the surface by a small fraction of their cells and the EPS matrix.[41] In particular, small biofilms are supported by very few cells, which are attached to the surface in vertical configuration.[41] Our nanowire sensor can thus be used to study the adhesion strength in this scenario. **Fig. 2F** shows the reconstructed 3D CLSM image data of a small biofilm adhered to our InP nanowire arrays (see also **Fig. S7** and **Supplementary video MV6**). The biofilm floating nature was clearly observable, with its structure connected to the surface through a few cells attached vertically to nanowires. The average adhesion force values for the nanowires marked in the bottom image in **Fig. 2F** were 50 - 90% larger than those observed for single, isolated cells in similar orientation (**Fig. 2G**, see also **Table S2**). The distribution of force values was also broader when the biofilm was present, and significantly higher than for single, vertical cells attached to the InP surface (**Fig. 2G**).

Additionally, we used these results to plot the magnitude and direction of the measured adhesion forces (**Fig. 2H**), and define the two most likely perpendicular directions of movement for each nanowire (blue and orange arrows in **Fig. 2H**). Here, we considered only data for deflection of both nanowires larger (+ 10%) than measured noise levels (for the control nanowire). These directions are also indicated in **Fig. 2I**, which shows a top CLSM image of the small biofilm. The inset shows that the isochronal movement of both nanowires occurred in a relatively narrow angular range. Furthermore, there is a non-negligible correlation (Pearson correlation coefficient $r = 0.66$) between the angular movements of both nanowires, suggesting that the movement of the entire biofilm can be tracked using this technique.

In order to investigate the role of the XadA1 adhesin on the initial adhesion process of *X. fastidiosa*, control experiments to localize the protein in bacterial cultures of the 9a5c citrus strain

were first carried out. In such experiments, wild type cells were grown on aminated flat InP surfaces; amine-functionalization was chosen in order to increase the overall cell adherence and to retain the biopolymers of interest on the surface after the labeling process, which removed most cells in irreversible adhesion stages. **Fig. 3 (A, B)** shows CLSM images of samples immunolabelled for XadA1 (green) and stained for cell membrane lipids (red). Small circular structures next to the remaining cells were visible (**Fig. 3A**), ranging in diameter from 190 to 600 nm. These structures present fluorescence emission in both green and red spectral regions, denoted by yellow in the merged images. In many cases, the green emission of XadA1 biomarker is more localized, as expected for proteins assembled in a lipid matrix. In fact, a few isolated spots (green emission only) were also observed in **Fig. 3A**. The circular shape of the structures, their spectral emission and the fact that they remained intact on the surface suggest the presence of OMV's loaded with XadA1.[44] Additionally, CLSM images in **Fig. 3B** also showed micrometer-sized rings, with more intense protein staining located at specific points on their surface, or their center. These rings are most likely remains of the soluble EPS, also containing lipids, which *X. fastidiosa* uses to eventually create a layered filamentous structure on the surface;[41] the soluble EPS is usually washed away during the immunolabeling process. **Fig. 3C**, in turn, shows results for the aminated nanowires, whose position is marked as a white dot in the merged images. The CLSM images suggest similar co-localization of lipids and XadA1 in circular structures, now adhered to the nanowires.

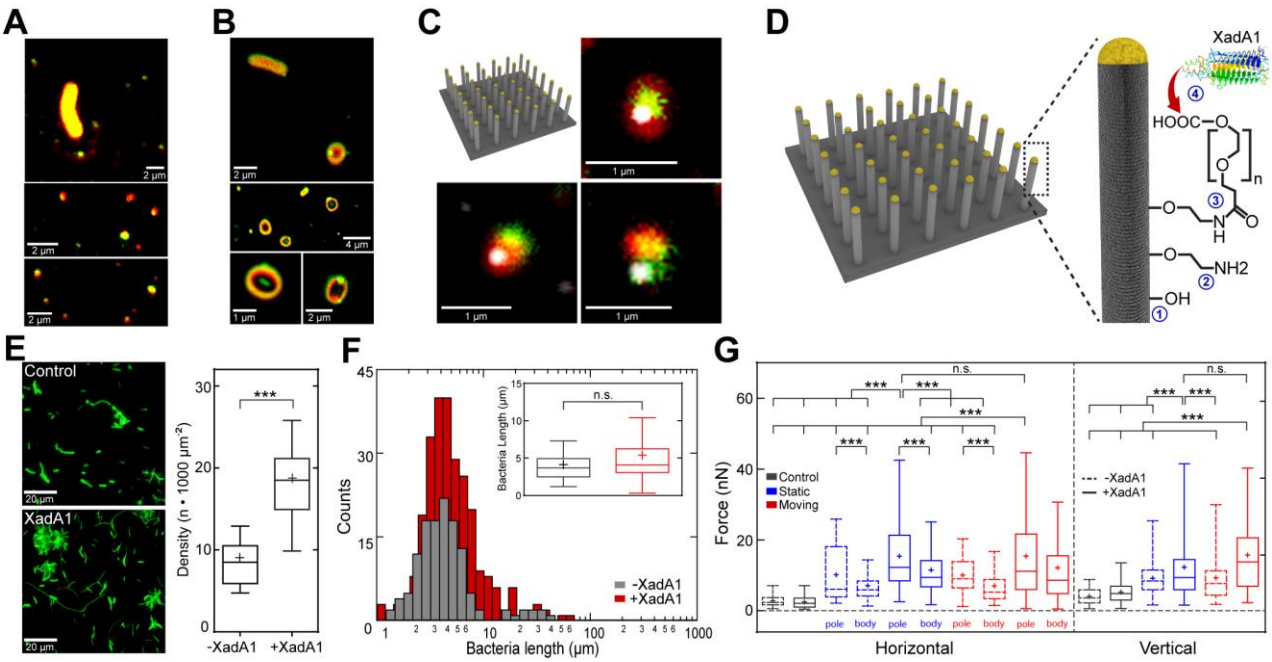

Figure 3. ***Ex-vivo*** **measurements on functionalized surfaces and nanowires.** CLSM images (**A, B**) of samples grown on flat, aminated InP substrates with labelled lipid (red) and XadA1 antibody (green) emissions overlapped. CSLM images (**C**) of samples grown on aminated InP nanowires (white), with labelled lipids (red) and XadA1 antibody (green) superimposed. Schematic representation (**D**) of the functionalization protocol for the InP nanowire array using PEG cross-linker and XadA1 adhesin. WFM images (**E**) of *X. fastidiosa* cells adhered to flat InP, control (–XadA1) and functionalized (+XadA1) surfaces; the Tukey boxplot shows the cell density in both cases ($n = 22$ images for each, –XadA1 and +XadA1, case), with statistically significant difference (two-tailed T-Test, significance level of $p=0.0001$). Cell length distribution (**F**) of adhered cells on the substrates (–XadA1, $n = 129$; +XadA1, $n = 267$) shown in (**E**); the inset shows the Tukey box plot. Overall force values (**G**) measured on functionalized surfaces compared to the original InP surface, shown as Tukey boxplots with the statistical results of applied one-way ANOVA and comparison via Tukey post-hoc test with $p = 0.0001$. All samples analyzed here were grown for 24 h prior to CLSM experiments. The statistics and number of cell adhesion forces measured for each configuration in (**G**) are summarized in **Table S1**.

Subsequently, the XadA1 adhesion protein for the citrus affecting strain was immobilized on both flat and nanowire array surfaces, as depicted in **Fig. 3D**. The chosen functionalization protocol is well established for XadA1[52,53] and several other biomolecules;[54,55] it includes the use of physically and chemically inert poly(ethylene glycol) cross-linker to suppress unspecific interactions between the substrate and bacteria.[56,57] Our *ex-vivo* measurements can then directly assess the impact of XadA1 on cell-surface interaction, mimicking its presence in OMVs released in living environment by the phytopathogen.[44] Indeed, immobilization of XadA1 on flat, control surfaces caused significant increase in overall *X. fastidiosa* cell surface adhesion efficiency. **Fig. 3E** shows WFM images of adhered, GFP-expressing cells on flat InP control (–XadA1) and functionalized (+XadA1) surfaces, and the corresponding density box plot. The presence of XadA1

on the surface leads to higher cell density; large cell lengths are observed for both populations (**Fig. 3F**), due to the filamentation process, which interconnects clusters.[41] These results strongly suggest that the protein is indeed a promoter of cell adhesion (see also **Fig. S8**). This hypothesis can be quantitatively investigated with our functionalized nanowire arrays.

Fig. 3G summarizes the forces measured for the several cell configurations considered previously, for both pristine (-XadA1) and functionalized (+XadA1) surfaces of nanowire arrays (**Supplementary videos MV7 to MV10**; the pristine, –XadA1, surfaces were only sterilized by chemical cleaning and O_2 plasma). In fact, our *ex-vivo* measurements were able to significantly resolve the forces for these two groups of experiments. Adhesin coating increased both average and maximum measured force values from 36 to 120%, depending on cell configuration. Larger differences from the control were observed for horizontal cells, both for polar and cell body regions. Furthermore, the XadA1-enriched surfaces also resulted in much larger distributions of *ex-vivo* force values, reaching up to 45 nN (see also **Table S1**).

Our force measurements have unequivocally determined an increase in adhesion strength when cells bind to XadA1-coated surfaces, corroborating indirect observations such as the increase in cell adhesion efficiency and filamentation shown in **Fig. 3E, F.** These results confirm the pivotal role of organochemical surface composition in regulating bacterial adhesion, growth and biofilm formation. The measured forces between InP nanowires and *X. fastidiosa* cells increase roughly two-fold for XadA1-coated surfaces, compared to the pristine InP samples. This increase in force is indeed related to the presence of adhesins on the surface since unspecific interactions between InP and bacterial cells were minimized by prior coating with poly(ethylene glycol) that renders the surfaces inert.[56-57] In fact, the force distribution values in presence of small biofilms (**Fig. 2G**) more closely resemble those obtained for single cells on surfaces that contain XadA1(**Fig. 3G**). Nevertheless, the larger forces measured on XadA1-coated nanowires can be attributed both to a larger adhesion strength due to the presence of adhesins and to a faster EPS production rate triggered by a stronger surface anchoring. Further studies are necessary to clarify this question in more detail.

From the biological point of view, however, our results contribute to the discussion on bacterial adhesion and host colonization mechanisms. Previous work has probed the interaction between XadA1 and several biotic and abiotic surfaces using force spectroscopy.[53] That work showed that inhomogeneously charged materials exhibited different binding characteristics for XadA1, which

in turn could be related to the different biofilm growth rates and morphological structures observed on corresponding surfaces.[53] Different adhesin binding characteristics upon attachment on different host surfaces can thus be expected. The release of XadA1-loaded OMV's in the extracellular media and subsequent surface deposition of the adhesin (as suggested by **Fig. 3A to C**) provide a mechanism for the bacteria to control adhesiveness to surfaces with very different chemical compositions and/or terminations, such as those of the hosts, plant and insect, where *X. fastidiosa* inhabits.[12,43,44,58,59] This seems particularly important for *X. fastidiosa*, due to its long cell division time and hence the need for a single cell to remain adhered to a surface for a longer period prior to cluster formation.

Recently, M. Ionescu *et al*.[44] have studied XadA1-loaded OMV's produced by *X. fastidiosa Temecula 1*, which infects grapevines. Mutant cells, which produce larger number of OMV's, were shown to be more virulent to plants and less adhesive to glass than wild type cells.[44] The authors thus hypothesized that *X. fastidiosa* cells bind to OMV's with lower efficiency than to surfaces where OMV's are found; the vesicles would block surface areas which would be available to the pathogen otherwise. The bacterial citrus strain used in our work is closely related to the grapevine's, since comparative analysis revealed that 98% of the genes and 95.7% of the amino acid sequences are shared by these two *X. fastidiosa* strains.[60] The authors of this genomic analysis concluded that the high similarity might indicate identical metabolic functions shared by these two microorganisms, which could likely use a common set of genes in plant colonization and pathogenesis, permitting convergence of functional genomic strategies. However, bacterial movement is slower in citrus plants,[61,62] suggesting that, in this case, cell adhesiveness may be intrinsically different from *X. fastidiosa Temecula 1*. In fact, the adhesin function might be strongly related to the pathogen-host interaction, which determines adaptation mechanisms towards the host colonization.

In summary, our results show a stronger adhesion force at the polar region of *X. fastidiosa* cells attached to the surface, confirming previous qualitative observations.[41] We also investigated the role of XadA1 TAA in the citrus-strain *X. fastidiosa* adhesion. Scattered vesicle-like, XadA1-loaded structures are found around adhered cells of the citrus strain in our static flow experiments. Moreover, XadA1 signatures are also present in larger size structures, reminiscent of early adhesion EPS disks, left over on the surface upon bacteria removal. The larger cell adhesion observed on XadA1-coated control surfaces, associated with the larger forces measured with

XadA1-functionalized nanowires, provide experimental, quantitative evidence to earlier suggestions that XadA1 is an important adhesion promoter for the citrus bacterial strain. Its release in OMVs can indeed be an important tool to modulate adhesion within the insect and plant hosts to *X. fastidiosa*, according to the particular needs of the pathogen life cycle. Moreover, bacteria that anchor biofilms to the surface demonstrate a stronger holdfast than single isolated cells, according to our measurements. To our knowledge, this is the first report on *ex-vivo* measurements of the adhesion force of a biofilm-anchoring bacterial cell. The present methodology has also proven feasible to further studies on biofilm elastic properties and movement within changing flow conditions (such as upon transmission between hosts), as indicated by the correlated movement of nanowires where the biofilm is anchored.

Furthermore, these results demonstrate the application of InP nanowire arrays as force sensors for bacterial cell adhesion. The methodology employed here can overcome bottlenecks in many conventional techniques, especially when environments similar to the host are considered. In addition, nanowire arrays with uniform size distribution within a chip provide the possibility to scan many cells within few seconds. Several parameters such as doping, stiffness and geometrical aspect ratios of the InP nanowires can be altered independently (**Fig. S9**) to thoroughly probe the different aspects of nanowire-bacteria interactions mechanisms, and to design unique pathways in engineering the biofilm structures for a variety of applications, such as antimicrobial surfaces and creating targets for new drugs.

ASSOCIATED CONTENT

Supporting Information. This article contains supporting information, such as material, methods, supplemental figures, movies and tables. This material is available free of charge via the Internet at http://pubs.acs.org.

AUTHOR INFORMATION

Corresponding Author

*Monica A. Cotta, Applied Physics Department, Institute of Physics 'Gleb Wataghin', State University of Campinas, 13083-859, Campinas, São Paulo, Brazil. Email: monica@ifi.unicamp.br

Author Contributions

P.K.S performed bacterial growth, sample preparations, FESEM imaging, WFM and CLSM experiments and data analysis. R.J. contributed with functionalization protocols, statistical data analysis and assembling the plots and figures. M.P.M. and D.M. carried out surface amination and labeling experiments, as well as WFM and CLSM measurements. A.C. processed the substrates and grew the nanowire arrays. M.V.M. and A.A.S. provided biological material and discussed the results from the microbiological point of view. C.L.C. discussed the setup for CLSM experiments. H.F.C. participated in the labelling experiments and, along with C.L.C., discussed the data obtained by CLSM. P.K.S., E.P.A.M.B. and M.A.C. designed the study. P.K.S., R.J. and M.A.C. wrote the article. M.A.C. supervised and managed the whole study. The manuscript was written through contributions of all authors. All authors have given approval to the final version of the manuscript.

ACKNOWLEDGMENT

The authors acknowledge J. H. Clerici, V.B. Pelegati and M. O. Baratti for technical assistance, and C.B. Santos and Prof. A.P.de Souza, from CBMEG/UNICAMP for providing the XadA1 protein. A.Cavalli and E.P.A.M. Bakkers would like to acknowledge Rene Van Veldhoven for the exceptional work and care for the MOVPE systems, and the technical support from the NanoLab@TU/e cleanroom. This work was financially supported by FAPESP (Fundação de Amparo a Pesquisa do Estado de São Paulo, Brazil), through grants 2010/51748-7 and 2013/02300-1, and CNPq (Conselho Nacional de Desenvolvimento Científico e Tecnológico, Brazil), grant number 479486/2012-3. D.M.M. and M.P.M. acknowledge scholarships from CAPES (Coordenação de Aperfeiçoamento de Pessoal de Nível Superior, Brazil); P.K.S. and R.J. acknowledge FAPESP for funding their scholarships. M.A. Cotta, A.A. de Souza and H.F. Carvalho acknowledge CNPq fellowships. The authors thank the access to confocal microscopy equipment provided by the National Institute of Science and Technology on Photonics Applied to Cell Biology (INFABIC) at the State University of Campinas; INFABIC is co-funded by FAPESP (08/57906-3) and CNPq (573913/2008-0). We also acknowledge the National Nanotechnology Laboratory (LNNano) at CNPEM, Brazil, for granting access to their electron microscopy facilities. A. Cavalli and E.P.A.M. Bakkers acknowledge the funding of the Dutch Technology

Foundation STW (Project 11826), which is part of the Netherlands Organisation for Scientific Research (NWO), and which is partly funded by the Dutch Ministry of Economic Affairs.

REFERENCES

1. Hall-Stoodley, L.; Costerton, J. W.; Stoodley, P. *Nat. Rev. Microbiology* **2004**, *2*, 95-108.
2. Flemming H-C.; Wingender, J. *Nat. Rev. Microbiology* **2010**, *8*, 623-633.
3. Danhorn, T.; Fuqua C. *Annu. Rev. Microbiol.* **2007**, *61*, 401–22.
4. Stewart, P. S.; Franklin, M. J. *Nat. Rev. Microbiology* **2008**, *6*, 199 -210.
5. Flemming, H-C.; Neu, T. R.; Wozniak, D. J. *J. Bacteriology* **2007**, *189*, 7945–7947.
6. Ducret, A.; Valignat, M-P.; Mouhamar, F.; Mignot, T.; Theodoly, O. *Proc. Natl Acad. Sci. USA* **2012**, *109*, 10036–10041.
7. Regina, V. R.; Lokanathan, A. R.; Modrzynski, J. J.; Sutherland, D. S.; Meyer, R. L. *PLoS ONE* **2014**, *9*, e105033.
8. Persat, A.; Nadell, C.D.; Kim, M. K.; Ingremeau, F.; Siryaporn, A.; Drescher, K.; Wingreen, N. S.; Bassler, B. L.; Gitai, Z.; Stone, H. A. *Cell* **2015**, *161*, 988-997.
9. Mikula, A.; Kolodziejczyk, R.; Goldman, A. *Frontiers in Cellular and Infection Microbiology* **2013**, *2*, 169.
10. Kaiser, P. O.; Riess, T.; Wagner, C. L.; Linke, D.; Lupas, A.N.; Schwarz, H.; Raddatz, G.; Schäfer, A.; Kempf, V. A. J. *Cellular Microbiol.* **2008**, *10*, 2223–2234.
11. Schluter, J.; Nadell, C. D.; Bassler, B. L.; Foster, K. R. *The ISME Journal* **2015**, *9*, 139–149.
12. Chatterjee, S.; Almeida, R. P.; Lindow, S. *Annu. Rev. Phytopathol.* **2008**, *46*, 243–71.
13. Bruinsma, G. M.; van der Mei, H. C.; Busscher, H. J. *Biomaterials* **2001**, *22*, 3217–3224.
14. Liu, Y.; Zhao, Q. *Biophysical Chemistry* **2005**, *117*, 39 – 45.
15. Pranzetti, A.; Mieszkin, S.; Iqbal, P.; Rawson, F. J.; Callow, M. E.; Callow, J. A.; Koelsch, P.; Preece, J. A.; Mendes P. M. *Adv. Mater.* **2013**, *18*, 2181-2185.
16. Saha, N.; Monge, C.; Dulong, V., Picart, C. & Glinel, K. *Biomacromolecules* **2013**, 14, 520–528.
17. Lichter, J. A.; Thompson, M. T.; Delgadillo, M.; Nishikawa, T.; Rubner, M. F.; Vliet, K. J. V. *Biomacromolecules* **2008**, *9*, 1571–1578.
18. Crawford, R. J.; Webb, H. K.; Truong, V. K.; Hasan, J.; Ivanova, E. P. *Adv. Colloid & Inter. Sci.* **2012**, 179–182, 142–149.
19. Rizzello, L.; Sorce, B.; Sabella, S.; Vecchio, G.; Galeone, A.; Brunetti, V.; Cingolani, R.; Pompa, P. P. *ACS Nano* **2011**, 5, 1865–1876.
20. Lorenzetti, M.; Dogsa, I.; Stosicki, T.; Stopar, D.; Kalin, M.; Kobe, S.; Novak, S. *ACS Appl. Mater. Inter.* **2015**, *7*, 1644−1651.
21. Diu, T.; Faruqui, N.; Sjostrom, T.; Lamarre, B.; Jenkinson, H. F.; Su, B.; Ryadnov, M. G. *Sci. Rep.* **2014**, *4*, 7122.
22. Hochbaum, A. I.; Aizenberg, J. *Nano Lett.* **2010**, *10*, 3717–3721.
23. Kim, P.; Epstein, A. K.; Khan, M.; Zarzar, L. D.; Lipomi, D. J.; Whitesides, G. M.; Aizenberg, J. *Nano Lett.* **2012**, *12*, 527–533.
24. Jeong, H. E.; Kim, I.; Karam, P.; Choi, H-J.; Yang, P. *Nano Lett.* **2013**, *13*, 2864–2869.
25. Sakimoto, K. K.; Liu, C.; Lim, J.; Yang, P. *Nano Lett.* **2014**, *14*, 5471–5476.
26. Wang, L.; Wang, H.; Yuan, L.; Yang, W.; Wu, Z.; Chen, H. *J. Mater. Chem.* **2011**, *21*, 13920-13925.
27. Wang, H.; Wang, L.; Zhang. P.; Tuan, L.; Yu, Q.; Chen, H. *Colloids and Surfaces B: Biointerfaces* **2011**, *83*, 355–359.
28. Tymchenko, N.; Wallentin, J.; Petronis, S.; Bjursten, L. M.; Kasemo, B.; Gold, J. *Biophysical Journal* **2007**, *93*, 335–345.
29. Lin, Y-C.; Kramer, C. M.; Chen, C. S.; Reich, D. H. *Nanotechnology* **2012**, *23*, 075101.
30. Hallstrom, W.; Lexholm, M.; Suyatin, D. B.; Hammarin, G.; Hessman, D.; Samuelson, L.; Montelius, L.; Kanje M.; Prinz, C. N. *Nano Lett.* **2010**, *10*, 782–787.
31. Zheng, X. R.; Zhang X. *J. Micromech. Microeng.* **2011**, *21*, 054003-13.

32. Ong,Y-L.; Razatos, A.; Georgiou, G.; Sharma. M. M. *Langmuir* **1999**, *15*, 2719-2725.
33. Potthoff, E.; Ossola, D.; Zambelli T.; Vorholt, J. A. *Nanoscale* **2015**, *7*, 4070 –4079.
34. Guillaume-Gentil, O.; Potthoff, E.; Ossola, D.; Franz, C. M.; Zambelli, T.; Vorholt, J. A. *Trends in Biotechnology* **2014**, *32*, 381-388.
35. Fallman, E.; Schedin, S.; Jass, J.; Andersson, M.; Uhlin, B. E.; Axner, O. *Biosensors & Bioelectronics* **2004**, *19*, 1429–1437.
36. Maier, B.; Potter, L.; So, M.; Seifert, H. S.; Sheetz. M. P. *Proc. Natl Acad. Sci. USA* **2002**, *99*, 16012–16017.
37. Tsang, P. H.; Li, G.; Brun, Y. V.; Freund, L. B.; Tang, J. X. *Proc. Natl Acad. Sci. USA* **2006**, *103*, 5764–5768.
38. Schoen, I.; Hu, W.; Klotzsch, E.; Vogel, V. *Nano Lett.* **2010**, *10*, 1823–1830.
39. Robinson, J. T.; Jorgolli, M.; Shalek, A. K.; Yoon, M -H.; Gertner, R. S.; Park, H. *Nat. Nanotech.* **2012**, *7*, 180–184.
40. Mansfield, J.; Genin, S.; Magori, S.; Citovsky, V.; Sriariyanum, M.; Ronald, P.; Dow, M.; Verdier, V.; Beer, S.V.; Machado, M. A.; Toth, I.; Salmond, G.; Foster, G. D. *Mol. Plant Pathol.* **2012**,*13*, 614–629.
41. Janissen, R.; Murillo, D. M.; Niza, B.; Sahoo, P. K.; Nobrega, M. M.; Cesar, C. L.; Temperini, M. L.; Carvalho, H. F.; de Souza A. A.; Cotta, M. A. *Sci. Rep.* **2015**, *5*, 9856.
42. Stokstad, E. *Sci. News* **2015**, *348*, 620.
43. Caserta, R.; Takita, M. A.; Targon, M. L.; Rosselli-Murai, L. K.; Souza, A. P.; Peroni, L.; Stach-Machado, D. R.; Andrade, A.; Labate, C. A.; Kitajima, E. W.; Machado, M. A.; de Souza, A. A. *Appl. Env. Microbiology* **2010**, *76*, 4250-4259.
44. Ionescu, M.; Zaini, P. A.; Baccari, C.; Tran, S.; Silva, A. M.; Lindow, S. E.; *Proc. Natl Acad. Sci. USA* **2014**, *111*, E3910-E3918.
45. Nascimento, R.; Gouran, H.; Chakraborty, S.; Gillespie, H.W.; Almeida-Souza, H.O.; Tu, A.; Rao, B.J.; Feldstein, P.A., Bruening, G.; Goulart, L.R.; Dandekar, A.M. *Sci Rep.* **2016**, 6, 18598.
46. Kulp, A.; Kuehn, M. J. *Annu. Rev. Microbiol*. **2010**, *64*, 163–184.
47. Turnbull, L.; Toyofuku, M.; Hynen, A. L.; Kurosawa, M.; Pessi, G.; Petty, N. K.; Osvath, S. R.; Carcamo-Oyarce, G.; Gloag, E. S.; Shimoni, R.; Omasits, U.; Ito, S.; Yap, X.; Monahan, L. G.; Cavaliere, R.; Ahrens, C. H.; Charles, I. G.; Nomura, N.; Eberl, L.; Whitchurch, C. B. *Nat. Comm.* **2016**, *7*, 11220.
48. Roier, S.; Zingl, F. G.; Cakar, F.; Durakovic, S.; Kohl, P.; Eichmann, T. O.; Klug, L.; Gadermaier, B.; Weinzerl, K.; Prassl, R.; Lass, A.; Daum, G.; Reidl, J.; Feldman M. F.; Schild, S. *Nat. Comm.* **2016**, *7*, 10515.
49. Schwechheimer, C.; Kuehn, M. J. *Nature Rev. Microbiology* **2015**, *13*, 605-619.
50. Hallstrom, W.; Martensson, T.; Prinz, C.; Gustavsson, P.; Montelius, L.; Samuelson, L.; Kanje, M. *Nano Lett.* **2007**, *7*, 2960-2965.
51. Ma, L.; Conover, M.; Lu, H.; Parsek, M. R.; Bayles, K.; Wozniak, D. J. *PLoS Pathogens* **2009**, *5*, e1000354.
52. Moreau, A. L. D.; Janissen, R.; Santos, C. A.; Peroni, L. A.; Stach-Machado, D. R.; de Souza, A.A.; de Souza, A. P.; Cotta, M. A. *Biosensors & Bioelectronics* **2012**, *36*, 62–68.
53. Lorite, G. S.; Janissen, R.; Clerici, J. H.; Rodrigues, C. M.; Tomaz, J. P.; Mizaikoff, B.; Kranz, C.; de Souza, A. A.; Cotta, M. A. *PLoS ONE* **2013**, *8*, e75247
54. Janissen, R.; Berghuis, B.A.; Dulin, D.; Wink, M.; van Laar, T.; Dekker, N.H. *Nucleic Acids Res.* **2014**, *42*, e137
55. Kühbach, K.; Hülsemann, M.; Herrmann, Y.; Kravchenko, K.; Kulawik, A.; Linnartz, C.; Peters, L.; Wang, K.; Willbold, J.; Willbold, D.; Bannach, O. *Front Neurosci.* **2016**, *10*, 8
56. Dang, Y.; Quan, M.; Xing, C-M.; Wang, Y-B.; Gong, Y-K. *J. Mater. Chem. B* **2015**, *3*, 2350-2361.
57. Shi, H.; Liu, H.; Luan, S.; Shi, D.; Yan, S.; Liu, C.; Li, R. K. Y.; Yin, J. *RSC Adv.* **2016**, *6*, 19238-19244.
58. Chatterjee, S.; Newman, K. L.; Lindow, S. E. *Mol. Plant Microbe Interact.* **2008**, *21*, 1309–1315.

59. Chatterjee, S.; Wistrom, C.; Lindow, S. E. *Proc. Natl Acad. Sci. USA* **2008**, *105*, 2670–2675.
60. Van Sluys, M.A. *et al. J. Bacteriol.* **2003**, *185*, 1018–1026.
61. Baccari, C.; Killiny, N.; Ionescu, M.; Almeida, R. P.; Lindow, S. E. *Phytopathology* **2014**, 1*04*, 27–33.
62. Niza, B.; Coletta-Filho, H. D.; Merfa, M.V.; Takita, M. A.; de Souza, A. A. *Plant Pathol.* **2015**, *64*, 1259–1269.

TABLE OF CONTENTS / ABSTRACT GRAPHICS

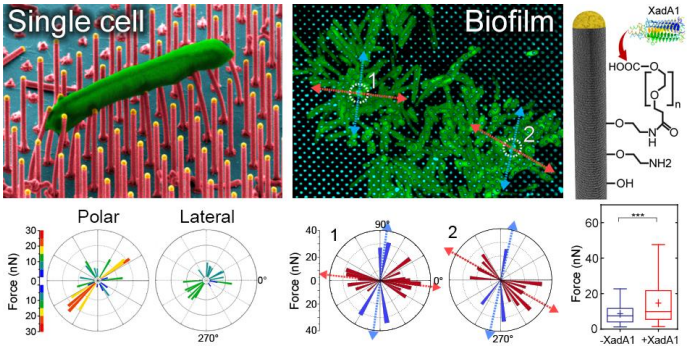

Supplemental Information

Material and Methods

Supporting figures and tables

Figure S1 *X. fastidiosa* cell size distribution
Figure S2 FESEM images (top view) of *X. fastidiosa* on flat InP surface and InP NW arrays
Figure S3 FESEM images of single *X. fastidiosa* cells adhered to InP nanowires
Figure S4 *Ex-vivo* CLSM-based force measurements of singly adhered *X. fastidiosa* cells
Figure S5 *Ex-vivo* forces of adhered *X. fastidiosa* single cells as a function of time
Figure S6 *Ex-vivo* force measurements for single cell with cell impact on nanowire
Figure S7 FESEM images of biofilm formed on nanowire arrays
Figure S8 *X. fastidiosa* cell adhesion on bare and XadA1-coated InP surfaces and NW arrays
Figure S9 Force calibration of InP nanowires as a function of NW length and diameter
Table S1 Adhesion force values obtained for all experimental conditions
Table S2 Adhesion forces of single cell biofilm anchors

Supporting movies (online)

Movie 1 Movement of single *X. fastidiosa* cells
Movie 2 Horizontally static single *X. fastidiosa* cells on NW arrays
Movie 3 Horizontal movement of single *X. fastidiosa* cells on nanowire (NW) arrays
Movie 4 Vertical movement of single *X. fastidiosa* cells on NW arrays
Movie 5 Vertically static single *X. fastidiosa* cells on NW arrays
Movie 6 *X. fastidiosa* biofilm 3D - rotating view
Movie 7 Horizontally static single *X. fastidiosa* cells on +XadA1 NW arrays
Movie 8 Horizontal movement of single *X. fastidiosa* cells on +XadA1 NW arrays
Movie 9 Vertical movement of single *X. fastidiosa* cells on +XadA1 NW arrays
Movie 10 Vertically static single *X. fastidiosa* cells on +XadA1 NW arrays

Material and Methods

Chemicals and reagents. All buffers and chemicals used in this study were purchased from Sigma-Aldrich, USA, unless otherwise mentioned therein.

Indium Phosphide nanowire array growth.

Nanowires were grown in a low-pressure Aixtron Closed Coupled Showerhead (CCS) MOVPE machine, with Hydrogen (H_2) used as carrier gas for precursors. The total flow was 6 l/min at a pressure of 50 mbar. Nanowires were grown on (111) InP substrates with the vapor-liquid-solid (VLS) method, in which Au droplets act as catalysts. 8 nm thick, 180 nm wide Au disks were patterned, with a square symmetry and a pitch of 513 nm, by nanoimprint lithography on a 2 inch wafer.[1] The 90 nm nanowire diameter was defined by the amount of Au catalyst. Before nanowire growth, an annealing step at 510 °C under PH_3/H_2 atmosphere was performed to remove organic residues from the nanoimprint process. Tri-methyl-indium (TMI) and phosphine (PH_3) were used as group III and V precursors. p-doped nanowires were obtained by doping in-situ by diethyl-zinc (DEZn) with a molar fraction of 6×10^{-6}. HCl was used in-situ to suppress tapering of the nanowires, with molar fraction constant during growth.[2] Growth times of p-doped nanowire were 18 min, after a short 1 min undoped stem.[3] Nanowires grew vertically, perpendicular to the substrate, in the <111> direction. The typical diameter and length of the nanowires in the array were 90 and 1500 nm, respectively. For bacterial adhesion studies, the substrates were cut into rectangular pieces of approximately 2 × 3 mm.

Substrate materials and cleaning process. For all conducted bacterial adhesion experiments, planar, undoped, (100)-oriented InP wafer substrates (AXT, USA), grown InP nanowire arrays and 22 x 22 mm borosilicate cover glasses (#0, Menzel GmbH, Germany) were cleaned to remove inorganic as well as organic contamination, and sterilized in a final step. To do so, the substrates were cleaned with acetone, isopropanol and deionized water, and dried with a gentle nitrogen flow. Prior to the bacterial adhesion studies, the substrates were sterilized by oxygen plasma (SE80, Barrel Asher Plasma Technology, USA) for 15 min (50 sccm O_2, 100 W, 100 mTorr).

Cloning, expression and purification of Xf.XadA1 membrane protein. The procedure used here was previously described in Moreau et al.[4] The *XF.XadA1* sequence ORF Xf1257 (3015bp), which encodes the *Xylella fastidiosa* surface adhesion protein Xf.XadA1 (1005 aa), was amplified from genomic DNA by PCR using specific primers. The "head" domain of Xf.XadA1, beginning at position 50 aa and ending at position 225 aa, was constructed using the primers $XF.XadA1_{forward}$ (5'-

CATAGCTAGCGGTCTTGCGCTTACAA-3‘) and XF.XadA1$_{reverse}$ (5‘-TGGAATTCGGCAATCG TCTTCACC-3’) containing the *Nhe*I and *Eco*RI restriction enzyme sites, respectively. The PCR amplification product was cloned into the expression vector pET28a(+) (Novagen, USA); an additional N-terminal six-histidines tag and a thrombin protease site to the coding sequence were included in this vector using the *Nhe*I and *Eco*RI restriction sites. The cloned domains were overexpressed in *E. coli* C43 (DE3) (Avidis) strain. Cells were grown at 37^{o} C in 1 liter of LB media, supplemented with 0.2% glucose and containing kanamycin (30 µg/mL) until optical absorbance of DO_{600} of 0.6–0.8 was reached. Recombinant proteins were induced by the addition of 1 mM IPTG (isopropyl-β-d-1-thiogalactopyranoside) followed by cultivation for 4 h at 25^{o}C and 200 rpm. The culture was harvested by centrifugation (3000 *g*, 15 min, 4 ^{o}C); sedimented cells were resuspended in 50 mL of buffer A (50 mm Tris-HCl, 150 mm NaCl, pH 8.0) plus 1 mg/mL lysozyme and 1 mM phenylmethanelsulfonylfluoride (Sigma, St Louis, USA) and incubated for 30 min on ice. The lysates were disrupted by sonication and the unbroken cells and debris were removed by centrifugation (27000 *g*, 40 min, 4^{o} C). The Xf.XadA1 protein purification was performed by affinity chromatography using a Ni-NTA column (Qiagen, Hilden, Germany), equilibrated with buffer A. The purified XadA1 proteins were eluted with five column volumes of buffer A containing 250 mM imidazole and the degree of purity was estimated by SDS-PAGE. Subsequently, the purification step the N-terminus His_6-tag of recombinant proteins were removed using a thrombin cleavage kit (Novagen, USA).

InP surface functionalization with XadA1 adhesin. The applied surface functionalization procedure is based on a previously described methodology[4] with minor modifications. Here, the cleaned and oxygen plasma treated InP substrates were incubated for 12 h in anhydrous DMSO (dimethyl sulfoxide) containing 5 M ethanolamine hydrochloride for surface amination. The substrates were then washed three times with deionized water and dried using a gentle nitrogen flow. These freshly prepared aminated substrates were further covalently PEGylated by incubation in amino-reactive heterobifunctional NHS-PEG-COOH (MW 3.400, LaysanBio, USA) in anhydrous chloroform containing 0.5 % (v/v) triethylamine for 1 h at room temperature. After the PEGylation process, the supports were washed five times with deionized water and dried with a gentle nitrogen flow. For covalent XadA1 protein attachment, 1 µM of the protein was added to the PEGylated InP substrates and bound via peptide binding in 100 mM MES (2-(N-morpholino)ethanesulfonic acid, pH 4.7) buffer containing 50 mM EDC (1-Ethyl-3-(3-dimethylaminopropyl)-carbodiimide) for 1 h reaction time at room temperature in humid atmosphere. After XadA1 immobilization, the substrates were washed five times with PBS buffer (pH 7.4) and immediately used for the bacterial adhesion studies. The 1 h

reaction time and several washing steps ensure the complete inactivation of EDC-activated carboxylic groups before *ex-vivo* bacterial experiments.[5,6]

Bacteria strains. *Xylella fastidiosa* wild type strain 9a5c and Green Fluorescent Protein (GFP) expressing strain 11399 were used in this study. Periwinkle Wilt broth (PW)[7] with Bovine Serum Albumin (BSA) was used as bacterial growth media.

Bacteria extraction and inoculum preparation. The extraction and growth of *X. fastidiosa* strains from Citrus variegated chlorosis (CVC) symptomatic sweet orange trees were conducted as previously described.[8,9] Harvested cells were resuspended in PBS (pH 7.4) buffer and the concentration was adjusted to OD_{600} = 0.3. Afterwards, the strains were grown in PW broth and incubated at 28°C for seven days in a rotary shaker at 180 rpm.

Bacterial growth. Bacterial inoculum in PW broth media with a concentration of 1×10^7 CFU mL^{-1} were used for all adhesion experiments. InP nanowire arrays (2 x 3 mm^2) were placed inside a custom made Teflon chamber (with 10 mm diameter and 5 mm in height) and 400 µl of inoculum were added. After covering the chamber with a sterilized borosilicate cover glass, the assembly was incubated inside a bacterial oven (410/3NDR, Nova Ética, Brazil) at 28 °C. After chosen growth times (24 h and 168 h), the whole system was taken for *ex-vivo* CLSM measurements. For scanning electron microscope studies, PW broth media was gently removed and the samples were washed three times with deionized water to completely remove the constituents of the culture media and non-attached biofilms; the samples were dried gently in nitrogen flow and temporarily stored at 4 - 8°C before measurements.

Polyclonal XadA1 antibody production. The *X. fastidiosa* polyclonal IgG antibody (Rheabiotech, Brazil) against XadA1 (further called anti-XadA1) was obtained by immunization of New Zealand White Rabbits based on the protocol of Caserta *et al.*[9] Briefly, 150 µg purified XadA1 proteins were mixed with Freund's complete adjuvant and injected into individual rabbits. The proteins solution was injected two more times, at 10 and 20 days after the first injection. The quality of the antibodies was verified by performing a direct ELISA (enzyme-linked immunosorbent assay), using the target XadA1 proteins as antigens and PBS as the negative control.

Immunolabeling of XadA1 adhesin. The immunofluorescence-based identification and localization of XadA1 adhesines was performed using polyclonal anti-XadA1 antibodies in combination with

Alexa488 conjugated secondary goat anti-rabbit IgG antibodies (#A11008, Invitrogen, USA). To do so, unfixed 9a5c bacteria strain samples with 24 h of growth at 28°C were washed twice for 5 min with phosphate-buffered saline (PBS, pH 7.4) to remove the constituents of the culture media and planktonic as well as non-attached clusters. In order to reduce unspecific adsorption of the antibodies, the samples were passivated with PBS/BSA buffer (PBS, containing 3% (w/v) BSA) for 1 h at room temperature. After washing the samples three times with PBS-T buffer (PBS, containing 0.01% (v/v) Tween20) for 2 min each, 10 $\mu g \cdot mL^{-1}$ of anti-XadA1 antibodies in PBS/BSA buffer were added to the samples and incubated for 1 h at 37°C. The samples were then washed twice for 10 min with PBS-T buffer and once with PBS buffer for 5 min. For fluorescence labeling of the anti-XadA1 antibodies, 1 $\mu g \cdot mL^{-1}$ of Alexa488-labeled secondary antibody was added to the samples in PBS/BSA buffer and again incubated for 1 h at 37°C, protected from light. In a final step, the samples were washed twice for 2 min with PBS-T buffer, twice with PBS buffer for 3 min and briefly with deionized water and then finally dried gently under nitrogen flow.

Lipid labeling process. For fluorescence-based labeling of lipid membranes, the commercial available PKH26 fluorescent linker kit was used (#P9691, Sigma). Lipid staining was carried out after XadA1 immunolabeling. To do so, 4 µM dye solution was added to the 9a5c bacterial strain samples and incubated for 5 min at room temperature. Afterwards, the samples were washed twice with deionized water and gently dried under nitrogen flow.

Wide-field epifluorescence microscopy. For the study of cell density adhered to flat InP substrate, the GFP-expressing bacteria strain 11399 samples were measured using an epifluorescence microscope (Nikon TE2000U, USA) with a peltier-cooled back-illuminated EMCCD camera ($IXON^3$, 1024 × 1024 pixels, Andor, Ireland) with 100× oil-immersion objective (CFI APO TIRF, NA. 1.45, Nikon, USA). A 150 W Mercury-lamp with appropriate filter sets (AHF, Tübingen, Germany) for GFP excitation and emissions were used to record the fluorescence images of bacteria. The reported number of bacteria identified on the InP substrate is based on the analysis of $n = 30$ measurements for 3 repetitions each.

Confocal laser scanning microscopy. Confocal Laser Scanning Microscopy (CLSM) measurements of bacteria adhered to nanowires and for immunolabeling studies on flat InP surface were carried out using a Zeiss LSM780-NLO confocal microscope (Carl Zeiss AG, Germany) with a 63× oil-immersion objective (Plan-Apochromat, NA. 1.4). The nanowire position and bacteria cells were simultaneously recorded from the 488 nm laser excitation in two different channels. The position of the individual nanowires of the arrays were captured from the reflection of laser line in one channel while the

localization of bacteria was performed by measuring the fluorescence emission of GFP (505 - 540 nm) in another channel. For analysis, the images were merged using ImageJ2 software.

The XadA1 distribution measurement via Alexa488-labeled secondary antibodies was examined using a laser line of 488 nm. Similarly, 651 nm laser excitation was used for lipid distribution imaging of the same samples via the PKH26 dye. All imaging was performed with pinholes set to 1 airy unit for each channel with 512 × 512 px (nanowire with bacteria) and 1024 × 1024 px (flat surface) image resolution and distances of 370 nm for the z-stack. The 3D-image analysis of the nanowire with bacterial and biofilm architecture was performed with ImageJ2/Fiji in combination with Imaris software (Bitplane, USA).[10] The reported observations were based on the analysis of $n > 50$ image acquisitions.

Scanning electron microscopy of bacterial cells on InP surface. The cell-surface interaction and cell adhesion density of *X. fastidiosa* cells, the EPS deposition and filament formation on different InP substrates were investigated using high-resolution FESEM (Field Emission Scanning Electron Microscopy; FEI Inspect F50). In order to preserve the cell integrity, EPS components and filament shapes, the samples were analyzed using low electron beam energy (1 keV) with short exposure times and secondary electron imaging mode. The use of Field Emission Gun (FEG) in the SEM system simultaneously provides high resolution and high contrast images with low electrostatic distortion, in general resulting in spatial resolution < 2 nm. For cell adhesion density analysis, $n > 100$ FESEM images were measured.

Image analysis. The measured time series of nanowire positions and cell positions were analyzed by ImageJ, ImageJ2/Fiji and Imaris software.[10] For each time series of cellular force measurements, the positions of all nanowire tips in a video frame were tracked by considering them as a solid circular particles; the center of the circle was computed from the position of horizontal and vertical Feret diameters of a circular post, automatically by appropriately choosing the range of particle size in the particle analysis plugin of ImageJ2/Fiji (**Fig S3**). The automated particle tracking analyzer module simultaneously analyzes and records the position of numerous objects and combines spots as they move through time. This plugin was also used to measure bacteria that move in space by diffusion or motility, to find the location of post appearances and disappearances, and to calculate the lifetime of post during a time series. The results were used for analysis of bacteria position and movement as well as for nanowire force changes in magnitude and orientation, for a chosen set of nanowires in each video frame. The 3D images of nanowire and bacteria/biofilm position were developed thereby combining the vertical tracking position of two different channels for the 3D viewer plugin in ImageJ.

Force calculations. The magnitude and orientation of the deflection of nanowires, determined from their tip positions in the times series, was analyzed using the ImageJ software and translated into forces. According to the linear elasticity theory for hexagonal cross-section,[12,13]

$$F = \frac{3EI}{L^3}\Delta x = \frac{15\sqrt{3}\,E\,D^4}{256\,L^3}\Delta x$$

where E depicts the Young's modulus of the nanowires, I corresponds to the second moment of inertia, D specifies the diameter of the nanowire, L identifies the length of the nanowire and Δx determines the displacement of the tip of the nanowire. The parameters for corresponding InP nanowire arrays used in this study are: D = 90 nm, L = 1500 nm, and Young's Modulus E = 106.4 GPa for InP (111).[14] It is important to emphasize that the nanowire diameter and length can be adjusted in order to probe a particular range of cellular forces (**Fig S8**).

Statistical analysis. For all employed statistical tests we used for the data selection Tukey's outlier filter of leveraging the Interquartile Range.[15] This method is applicable to most ranges since it does not depend on distributional assumptions. It also ignores the mean and standard deviation, making it resistant to being influenced by the extreme values in the range. Bacterial density and length values as well as the described nanowire force distributions were plotted as Tukey box plots considering the described outlier filter. The statistical tests to analyze differences in bacterial density and length as a function of InP surface composition was performed using two-tailed t-test with a significance level of $p = 0.0001$. Cellular adhesion forces exerting on nanowires dependent on InP surface composition, cell orientation and movement were analyzed using one-way two-tailed analysis of variance (ANOVA, $p = 0.0001$) with subsequent Tukey post-hoc test for statistical comparison.

Supporting figures and tables

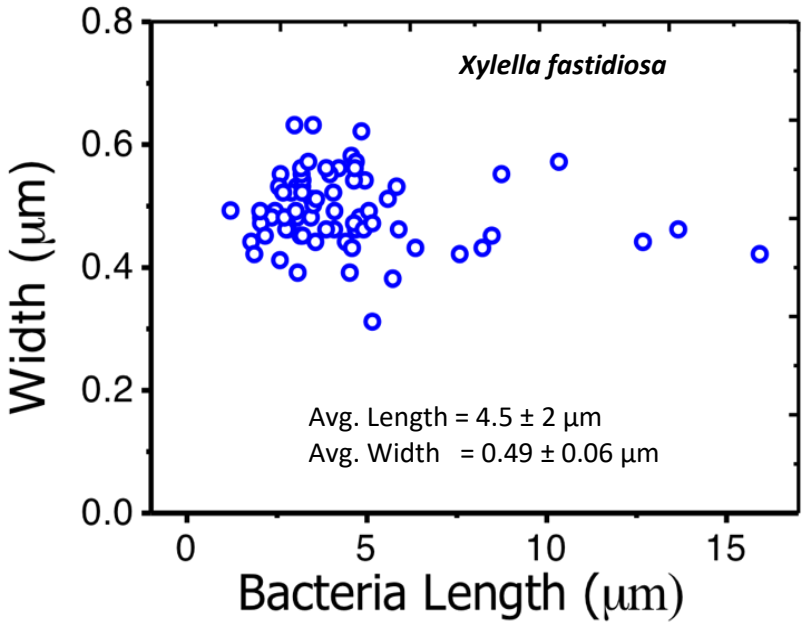

Figure S1. Size distribution of *X. fastidiosa* cells obtained from FESEM and WFM images. Average length and width are shown as inset. The longer cells are due to filamentation taking place in between clusters.[8]

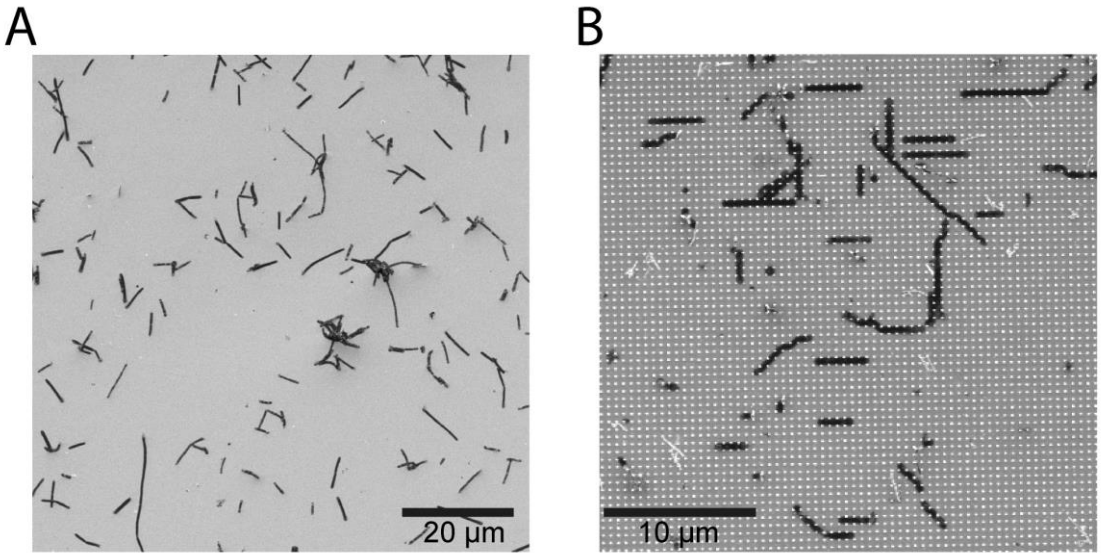

Figure S2. Large scale FESEM images of dry *X. fastidiosa* cells on (**A**) flat InP substrate and (**B**) InP nanowire arrays. The alignment of bacteria following the nanoscale topography is clearly observable; cells are attached within the vicinity of nanowires in the array.

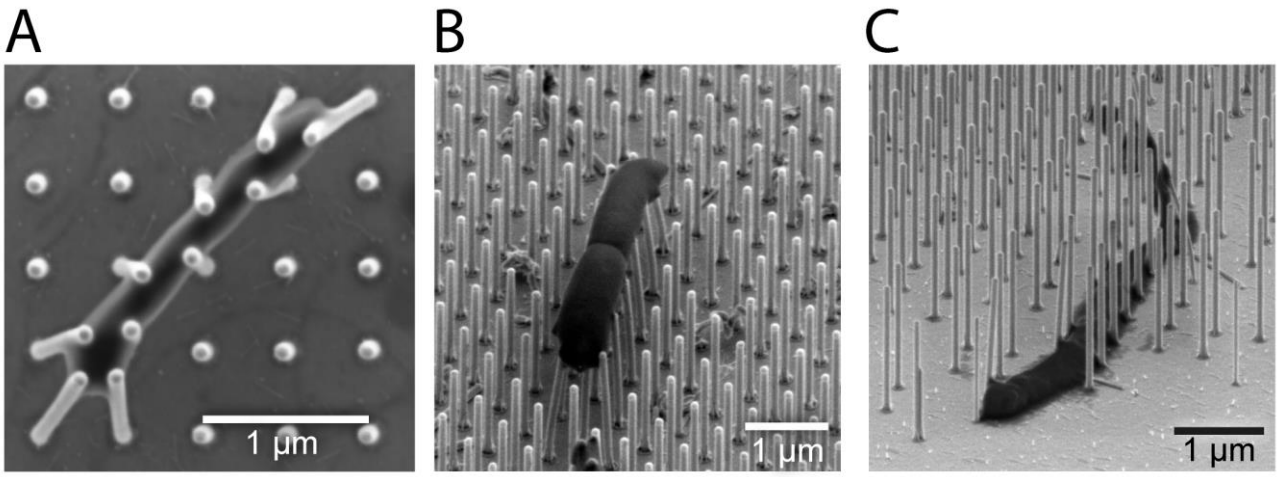

Figure S3. FESEM images of single *X. fastidiosa* cells on InP nanowire arrays. Perpendicular view (**A**) of a cell trapped by nanowire arrays, most likely via the secreted EPS matrix. Two daughter cells (**B**) attached on the top of the nanowire arrays. Cells on the bottom surface (**D**) within nanowire vicinity in the array.

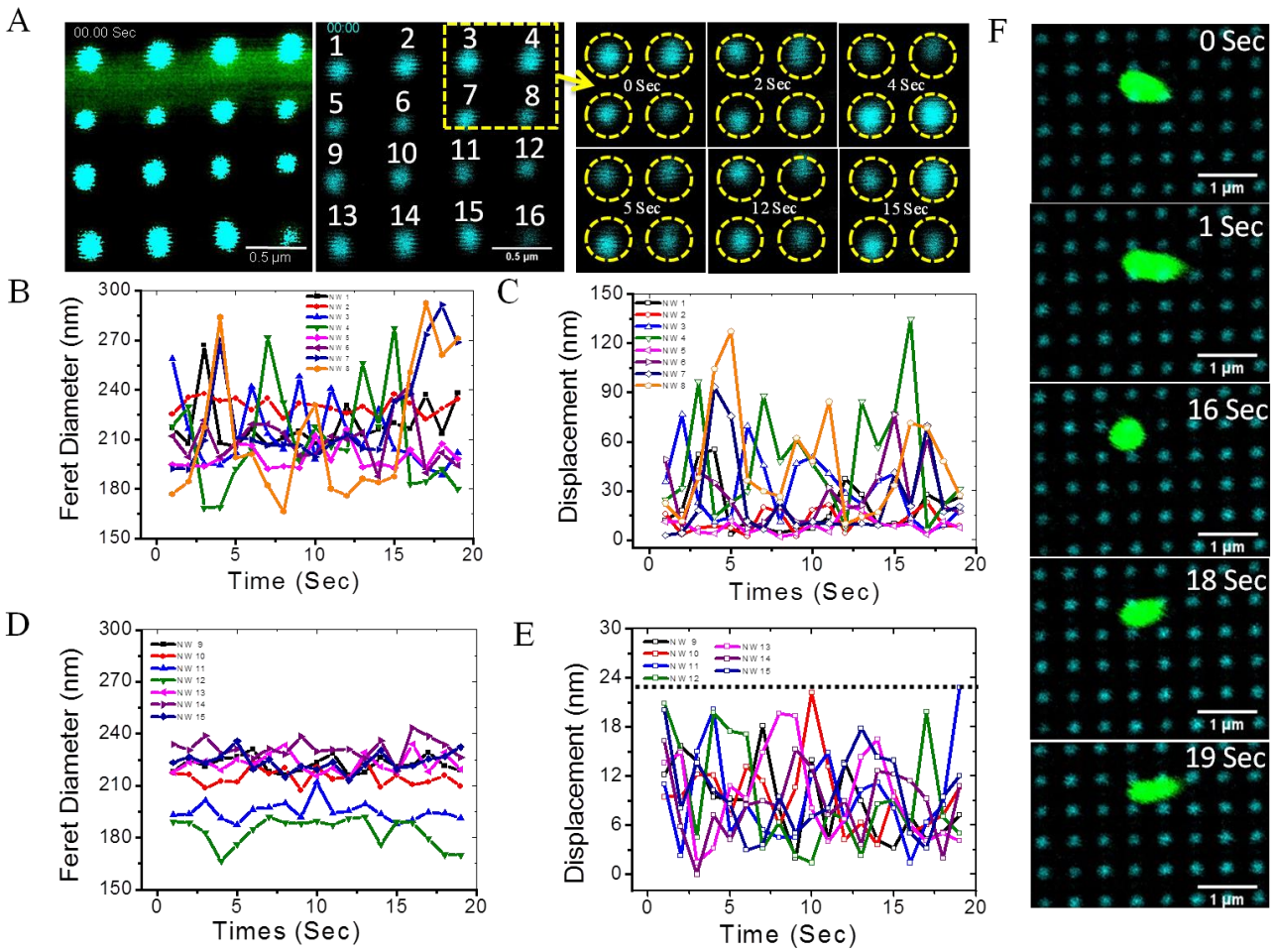

Figure S4. *Ex-vivo* force measurements for single cells. The CLSM images show *X. fastidiosa* cells adhered to InP nanowires (the images show the fluorescence of GFP and the reflected laser intensity at the nanowire tip). Bacteria attached horizontally (**A**) on nanowire arrays (moving) and selected region (yellow dotted Square; middle) shows how the nanowire top position changes upon bacterial movement (right side), and time series of Feret diameters (**B**, **D**) and nanowire displacements (**C**, **E**) extracted from CLSM videos: (**B**, **C**) nanowires with bacteria attached and (**D**, **E**) nanowires without bacteria (used as control for the experiment). The dashed line in (**E**) indicates the displacement associated with the noise limit force value (5 nN).similarly (**F**) a vertically attached bacteria (moving) and their temporal position recorded form the captured video.

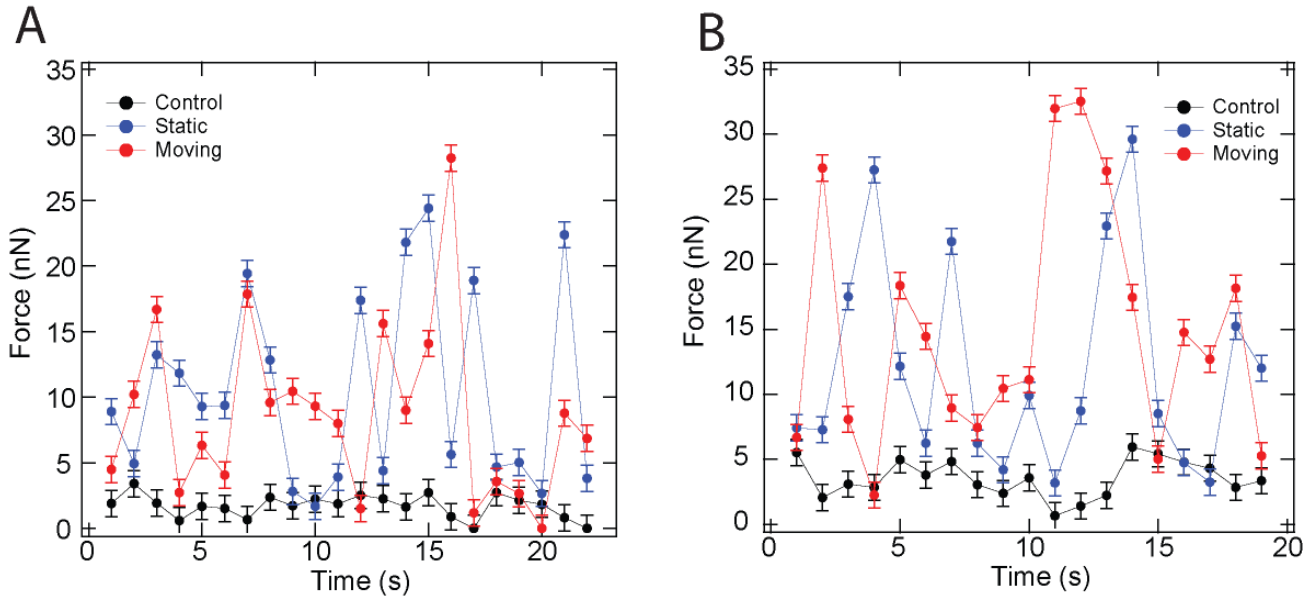

Figure S5. *Ex-vivo* force measurements for single cells. The graphs show the change in forces over time for control nanowires (black), static (blue) and moving (red) adhered bacterial cells in the horizontal (**A**) and vertical (**B**) configurations. The large fluctuations are mainly due to the 'stroboscope' effect caused by the slow laser scanning rate, when compared to the faster nanowire motion.

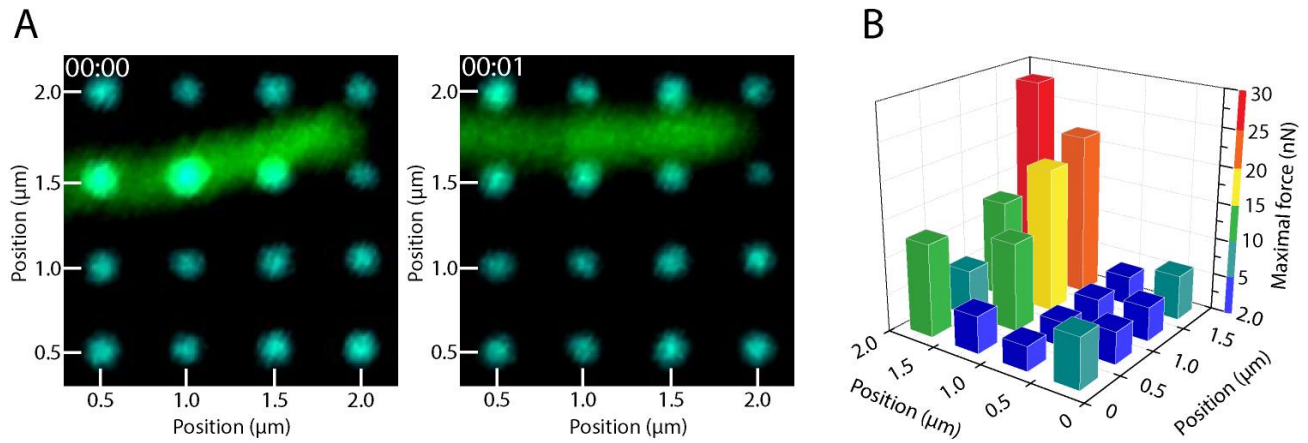

Figure S6. *Ex-vivo* force measurements for single cells. Recorded video frames (**A**) show the movement of bacterial cell with pole adhered to nanowire outside the image field of view. Corresponding maximum force values (**B**) observed for each nanowire in the image (**A**).

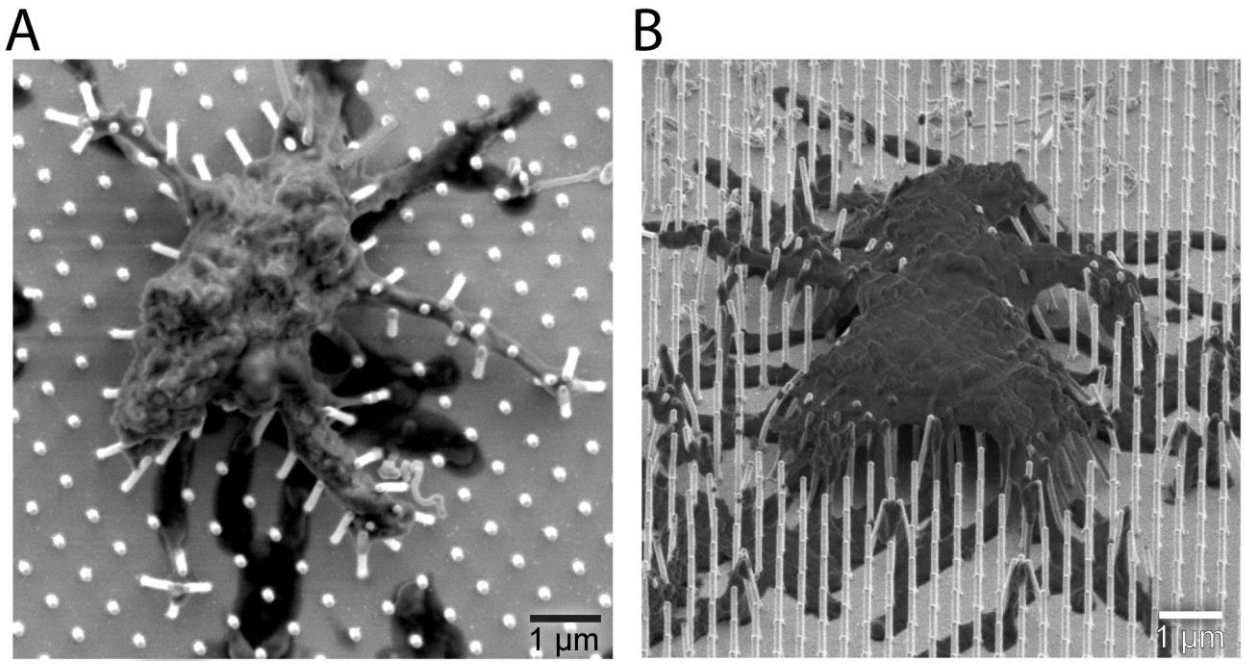

Figure S7. FESEM images of dry, small biofilms on InP nanowire array in perpendicular (**A**) and tilted (**B**) view. The EPS matrix covering the biofilm strongly contributes to its integrity and surface adhesion strength.

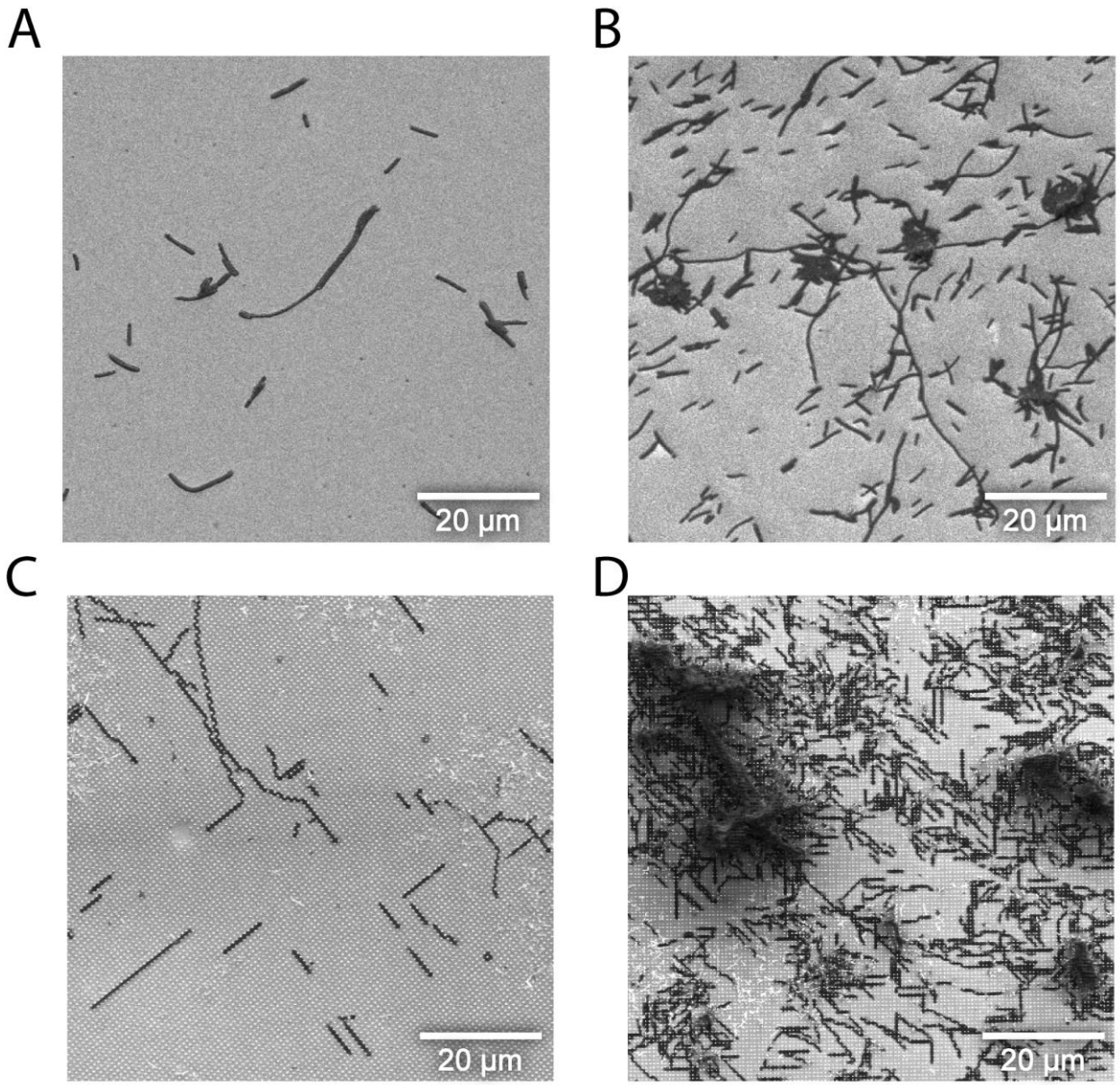

Figure S8. FESEM images of dry *X. fastidiosa* bacterial cells attached to (**A**) flat InP substrate and (**B**) flat XadA1-coated InP substrate, with same growth times. Corresponding cell distributions on InP nanowire arrays for non-coated (**C**) and XadA1-functionalized (**D**) InP nanowire array. The results indicate that the bacterial cell densities increase significantly upon functionalization with XadA1 and consequently the rapid formation of biofilms.

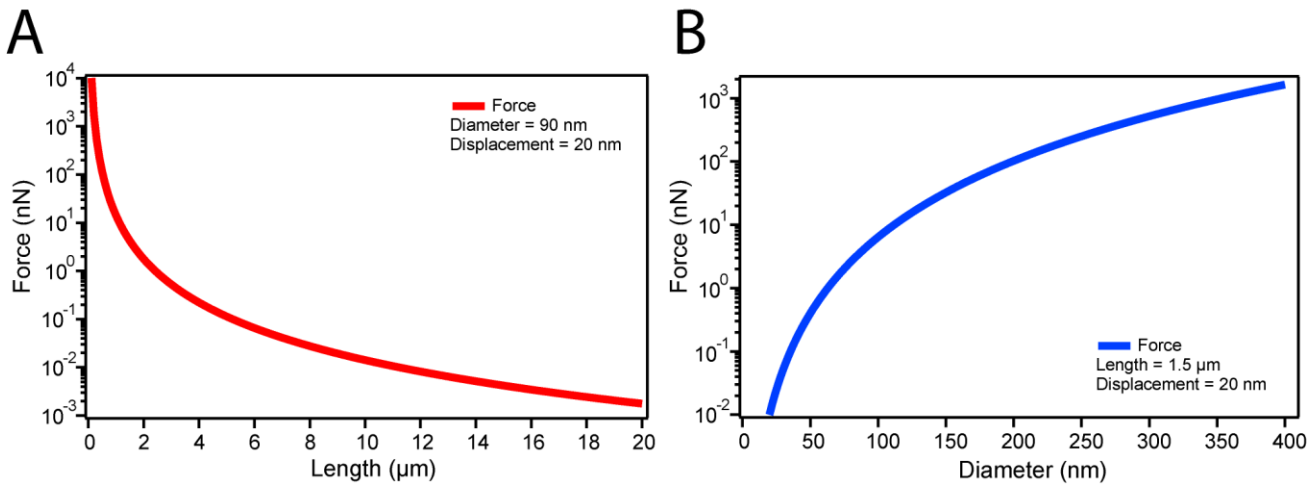

Figure S9. Calculations showing the possibility of measuring the range of bacterial adhesion forces by appropriately choosing (**A**) length and (**B**) diameter of InP nanowire arrays. The calculations show that these arrays have the potential to measure a wide range of forces - from pN to nN – from bacterial cells. The minimum nanowire tip displacement observable in CLSM measurements was considered for the calculations.

Table S1. Average and maximum adhesion force values (in nN) of single cells obtained for all experimental conditions, such as horizontally (H) and vertically (V) moving (M) and static (S) cells on bare and XadA1 (X) coated InP nanowire arrays. For horizontal oriented cells, forces from the bacterial pole and cell body are described with *P* and *B*, respectively. The force values correspond to the Tukey plot shown in Figure 3G. Obtained forces of control nanowires for every condition are denoted with C.

		Configuration	***N***	**Average ± *SD***	**Median**	**F_{max}**
Horizontal	Control	HC	222	2.6 ± 1	2.3	7.3
		HCX	256	2.7 ± 2	2.2	7.5
	Static	HS*P*	137	10.2 ± 8	6.1	25.8
		HS*B*	130	7.1 ± 4	5.7	13.6
		HSX*P*	159	15.4 ± 10	12.3	42.2
		HSX*B*	144	11.5 ± 7	9.4	25.1
	Moving	HM*P*	65	10.1 ± 5	9	20.3
		HM*B*	137	6.9 ± 5	5.3	16.7
		HMX*P*	164	15.2 ± 12	11.1	45.4
		HMX*B*	144	12.2 ± 10	8.7	31.9
Vertical	Control	VC	123	4 ± 2	3.6	8.9
		VCX	193	5.3 ± 3	4.9	13.8
	Static	VS	113	9 ± 5	8.4	25.5
		VSX	172	12.3 ± 9	9.4	43.2
	Moving	VM	92	8.6 ± 6	7.3	30.2
		VMX	141	15.8 ± 10	13.8	41

Table S2. Average and maximum adhesion force values (in nN) of single cells that anchors the biofilm shown in Figure 2 G.

	Control	Nanowire 1	Nanowire 2
N	42	42	42
Average *SD*	4.6 ± 3	17.1 ± 10	14.2 ± 10
Median	5.1	15.9	9.8
F_{max}	10.2	34.5	32.6

References

1. Martensson, T.; Carlberg, P.; Borgstrom, M.; Montelius, L.; Seifert, W.; Samuelson L. *Nano Lett.* **2004**, *4*, 699–702.
2. Borgstrom, M. T.; Wallentin, J.; Tragardh, J.; Ramvall, P.; Ek, M.; Wallenberg, L. R.; Samuelson, L.; Deppert, K. *Nano Res.* **2010**, *3*, 264–270.
3. Gao, L.; Cui, Y.; Wang, J.; Cavalli, A.; Standing, A.; Vu, T. T. T.; Verheijen, M. A.; Haverkort, J. E. M.; Bakkers, E. P. A. M.; Notten, P. H. L. *Nano Lett.* **2014**, *14*, 3715–3719.
4. Moreau, A. L. D.; Janissen, R.; Santos, C. A.; Peroni, L. A.; Stach-Machado, D. R.; de Souza, A.A.; de Souza, A. P.; Cotta, M. A. *Biosensors & Bioelectronics* **2012**, *36*, 62–68.
5. Jacobson, B.S.; Fairman, K.R. *Anal. Biochem.* **1980**, *106*, 114-117.
6. Hermanson, G.T. Bioconjugate Techniques (Academic Press: Amsterdam, **2013**)
7. Davis, M. J.; French, W. J.; Schaad, N. W. *Current Microbiology* **1981**, *6*, 309–314.
8. Janissen, R.; Murillo, D. M.; Niza, B.; Sahoo, P. K.; Nobrega, M. M.; Cesar, C. L.; Temperini, M. L.; Carvalho, H. F.; de Souza A. A.; Cotta, M. A. *Sci. Rep.* **2015**, *5*, 9856.
9. Caserta, R.; Takita, M. A.; Targon, M. L.; Rosselli-Murai, L. K.; Souza, A. P.; Peroni, L.; Stach-Machado, D. R.; Andrade, A.; Labate, C. A.; Kitajima, E. W.; Machado, M. A.; de Souza, A. A. *Appl. Env. Microbiology* **2010**, *76*, 4250-4259.
10. Schneider, C. A.; Rasband, W. S.; Eliceiri, K. W. *Nat. Methods* **2012**, *9*, 671–675.
11. Landau, E. D.; Lifshizt, E. M. Theory of Elasticity (Pergamon Press: New York, **1959**).
12. Hallstrom, W.; Lexholm, M.; Suyatin, D. B.; Hammarin, G.; Hessman, D.; Samuelson, L.; Montelius, L.; Kanje M.; Prinz, C. N. *Nano Lett.* **2010**, *10*, 782–787.
13. Landau, E. D.; Lifshizt, E. M. Theory of Elasticity (Pergamon Press: New York, **1959**).
14. Santos, C. L.; Piquini, Paulo. *Phys. Rev. B* **2010**, *81*, 075408.
15. Frigge, M.; Hoaglin, D. C.; Iglewicz, B. *The American Statistician* **1989**, *43*, 50–54.